Chapter

Processing Techniques with Heating Conditions for Multiferroic Systems of $BiFeO_3$, $BaTiO_3$, $PbTiO_3$, $CaTiO_3$ Thin Films

Kuldeep Chand Verma and Manpreet Singh

Abstract

In this chapter, we have report a list of synthesis methods (including both synthesis steps & heating conditions) used for thin film fabrication of perovskite ABO_3 ($BiFeO_3$, $BaTiO_3$, $PbTiO_3$ and $CaTiO_3$) based multiferroics (in both single-phase and composite materials). The processing of high quality multiferroic thin film have some features like epitaxial strain, physical phenomenon at atomic-level, interfacial coupling parameters to enhance device performance. Since these multiferroic thin films have ME properties such as electrical (dielectric, magneto-electric coefficient & MC) and magnetic (ferromagnetic, magnetic susceptibility etc.) are heat sensitive, i.e. ME response at low as well as higher temperature might to enhance the device performance respect with long range ordering. The magnetoelectric coupling between ferromagnetism and ferroelectricity in multiferroic becomes suitable in the application of spintronics, memory and logic devices, and microelectronic memory or piezoelectric devices. In comparison with bulk multiferroic, the fabrication of multiferroic thin film with different structural geometries on substrate has reducible clamping effect. A brief procedure for multiferroic thin film fabrication in terms of their thermal conditions (temperature for film processing and annealing for crystallization) are described. Each synthesis methods have its own characteristic phenomenon in terms of film thickness, defects formation, crack free film, density, chip size, easier steps and availability etc. been described. A brief study towards phase structure and ME coupling for each multiferroic system of $BiFeO_3$, $BaTiO_3$, $PbTiO_3$ and $CaTiO_3$ is shown.

Keywords: thin films synthesis, magnetoelectric coupling, film-on-substrate geometry

1. Introduction

Multiferroics have simultaneous ferroelectric and magnetic ordering and exhibits unusual physical properties in the sense of heat transport phenomenon at low and higher temperature turns to identify new device applications of spintronics due to their coupling between dual order parameters [1–6]. The first

magnetoelectric (ME) effect studied by Dzyaloshinskii on Cr_2O_3 in 1960s was discussed in the report [2]. After few decades, the study has been taken on bulk composites of magnetostrictive ferrites and piezoelectric $BaTiO_3$. But the research was halted during number of years due to observed weak value of ME coupling. Now around 2003, the spin-dependent multiferroicity and strong ME effect in $TbMnO_3$ has been reported and the coexistence of antiferromagnetism and ferroelectric polarization in $BiFeO_3$ (BFO) have created much interest in multiferroics [3]. Such perovskite BFO sure multiferroicity due to the fact that magnetism requires unpaired d^n cations, while ferroelectricity due to d^0 configuration.

1.1 Mechanism of multiferroicity (heat sensitive electric and magnetic behavior) occur in perovskites structure

The ME effect in multiferroic is caused due to switching of magnetization M with an applied electric field E and vice-versa. Moreover, multiferroic switching states should remain (a "persistent" switch, not a transient), and be fast [6]. In single phase multiferroics, the ferroelectricity and ferromagnetism created due to same structural arrangement in ABO_3 like $BiFeO_3$, $BaTiO_3$, $PbTiO_3$, $CaTiO_3$ etc., *i.e.* either due to same ion (e.g. Fe^{3+}) and or the ferroelectricity arises due to one ion (e.g. the unpaired electron in Pb or Bi), while the magnetism via a second ion (e.g. Fe in $BiFeO_3$). For memory devices, it is desired that the multiferroic to be highly insulating and function at room temperature with a large switching charge. For a MERAM, it is likely to combine the ultrafast (250 ps) electrical WRITE operation with the non-destructive (no reset) magnetic READ operation, *i.e.* combining the best qualities of FRAM and MRAM. However, the magnetization may small for an effective READ.

1.2 Multiferroic heterostructure

The multiferroic heterostructures is actually the thin film form of the multiferroic. For this, **Figure 1** shown the electric field control and switch of the local magnetism which has two coupling mechanisms exists in ferromagnet-multiferroic heterostructure [4]. In addition to the macroscopic stress, the heteroepitaxy (the growth of a material B on a different material A) caused an intrinsic epitaxial stress so that the crystal symmetry, lattice constant, and/or chemical bonds do not matched perfectly. During the start of the films growth, the substrate lattice constants might to form stresses. Besides to the single-phase multiferroic such as $BiFeO_3$, $BaTiO_3$, $PbTiO_3$, $CaTiO_3$, the composite multiferroic heterostructures constructed in the way to realize an artificial systems in the form of thin film. Wang *et al.* [3] reported an enhancement of polarization in heteroepitaxially constrained $BiFeO_3$ thin film which display a room-temperature spontaneous polarization (50 to 60 μC cm^{-2}) that is much higher (in magnitude) than from bulk (6.1 μC cm^{-2}). The films thickness is also play an important role to turn multiferroicity in heterostructure.

1.3 Strain mediated magnetoelectric effects

The ME coupling in two-phase multiferroics is the strain transfer phenomenon occurs among two phases which is schematically constructed for 1–3 nanocomposite (**Figure 2**) [5]. It is the polarization (magnetization) that changed by a magnetic (electric) field. The ME effect in composites is a product tensor property of the magnetostrictive or magnetoelastic effect (magnetization and lattice strain coupling) in one phase and the piezoelectric effect (polarization and lattice strain

DOI: http://dx.doi.org/10.5772/intechopen.101122

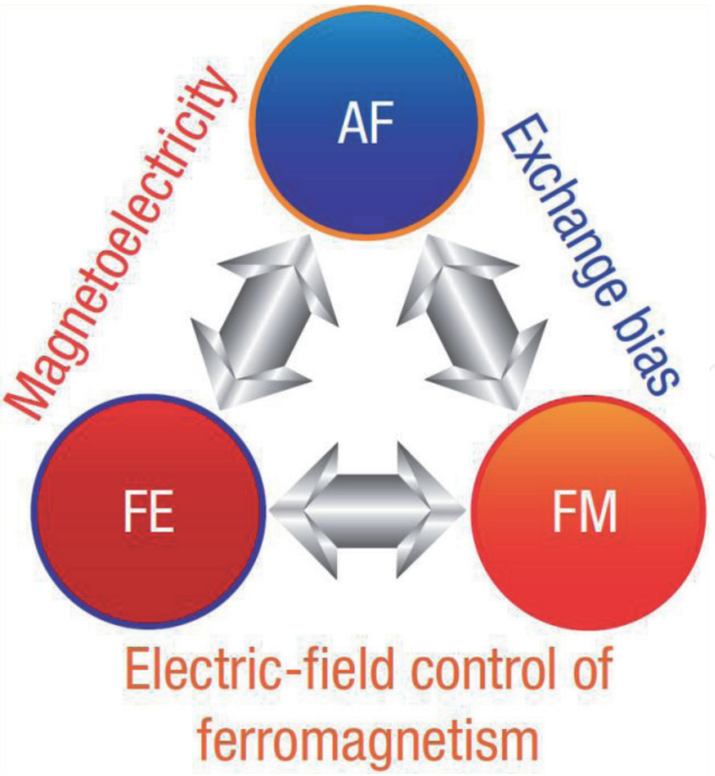

Figure 1.
Representation (schematic) of electric control of magnetism due to existence of ferroelectricity, antiferromagnetism and ferromagnetism [4].

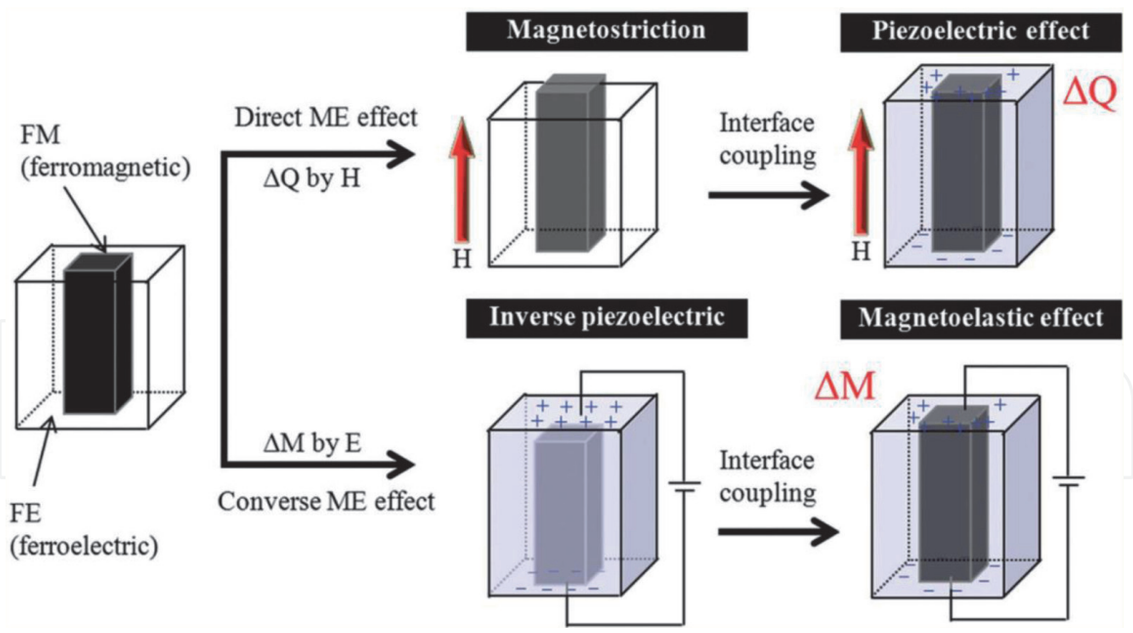

Figure 2.
Strain-mediated ME coupling in composites of a ferromagnetic (FM) and a ferroelectric (FE) phases (ΔQ: induces surface charges and ΔM: induces a magnetization change or domain reorientation) [5].

coupling) in the other phase. This ME coupling is the measurement due to direct or converse ME coefficient which detects an electrical signal with applied magnetic field. The strain generated in the magnetostrictive phase by a magnetic field induces surface charges in the piezoelectric phase. The direct ME voltage coefficient is given by $\alpha_E = \Delta E/\Delta H_{ac}$.

2. Multiferroic perovskite thin films and their processing techniques

2.1 $BiFeO_3$

Recently, the multiferroic systems such as $BaTi_2O_4$, $YMnO_3$, $BiMnO_3$, $LuFe_2O_4$, and $BiFeO_3$ have been widely investigated [7]. Among them, $BiFeO_3$ (BFO) with high $T_c \sim 1103$ K and $T_N \sim 643$ K attracts much attention due to its simultaneous ferroelectric and antiferromagnetic behaviors exist even at room temperature. This BFO has ferroelectricity occurs due to $6s^2$ lone pair of electrons of Bi^{3+} where structural distortion take-place and the magnetism occurs via superexchange interactions in Fe-O-Fe ions [8, 9]. This suggested to the polarization enhancement in BFO via chemical substitution along A site from rare-earth such as La^{3+}, Sm^{3+}, and Dy^{3+} ions due to their similar ionic radius and isovalent chemistry with Bi. This substitution of rare-earth into Bi in BFO may also induce a reduction in T_c value and formation of an antiferroelectric phase, but had minimal effect on antiferromagnetism. Moreover, the magnetization in BFO resulted by G-type antiferromagnet order is a cycloidal of wavelength, $\lambda \sim 62–64$ nm [10].

2.1.1 Multiferroic $BiFeO_3$ thin film

The bulk $BiFeO_3$ is a room-temperature ferroelectric with a spontaneous electric polarization directed along one of the [111] axes in the perovskite structure as shown in **Figure 3a** [11]. The ferroelectricity due to lattice distortions reduces the symmetry from cubic to rhombohedral to cause ferroelastic strain. With applied an electric field, the ferroelectric polarization in $BiFeO_3$ have eight possible positive

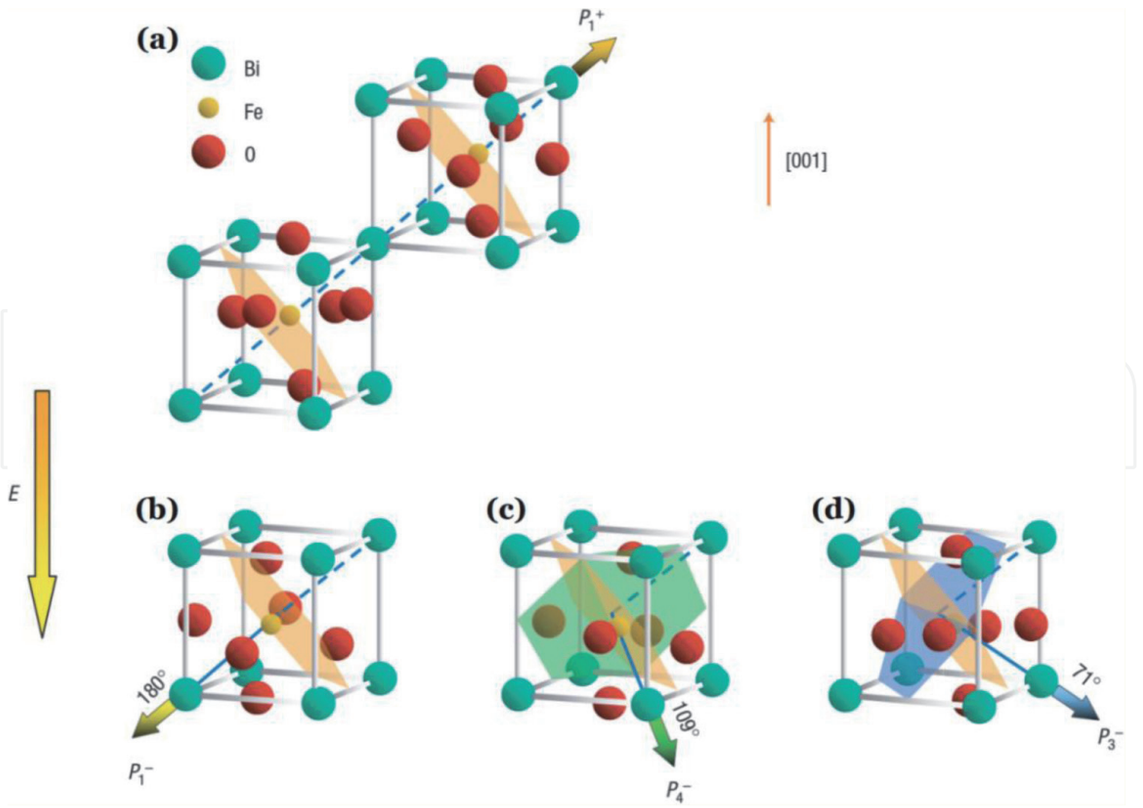

Figure 3.
The (001)-oriented $BiFeO_3$ crystal structure (schematic) and the ferroelectric polarization (bold arrows) and antiferromagnetic plane (shaded planes). (a) Polarization with an up out-of-plane component before electrical poling. (b) 180° polarization switching with the out-of-plane component switched by an electrical field (no change in antiferromagnetic phase). 109° (c) and 71° (d) polarization switching with the out-of-plane by an electrical field (antiferromagnetic plane changes) [11].

and negative orientations along the four cube diagonals, and the direction of the polarization can be switched by 180°, 109° and 71° as shown in **Figure 3b–d**. Switching of the polarization by either 109° or 71° changes the rhombohedral axis in the lattice system due to switching of the ferroelastic domain state. The antiferromagnetic ordering is G-type for which the nearest neighbor Fe moments aligned antiparallel to each other. In bulk $BiFeO_3$, the orientation of the antiferromagnetic vector has a long-wavelength spiral, which may suppress in thin films [12]. The DFT first principle calculations suggested the preferred orientation of the individual spins, in the absence of the spiral, which is perpendicular to the rhombohedral axis. It results into polarization switching by either 71° or 109° that should change the orientation of the easy magnetization plane. **Figure 1d** is the ferroelectric switching with 71° which leads to a reorientation of the antiferromagnetic order results into ME switching effects expectable in BFO films.

2.1.2 Synthesis techniques for $BiFeO_3$ thin films

In **Table 1**, we have included a lot of study to summarize chemical synthesis routes for processing of multiferroic $BiFeO_3$ thin films. The observed values of grain size, thickness and quality of film might be depends upon material processing and film coating technique.

2.2 $BaTiO_3$

$BaTiO_3$ (BTO) has shown multiferroicity at room temperature [36]. The three lattice structural phases of BTO are ferroelectric: rhombohedral<190 K, orthorhombic for 190 K < T < 278 K and tetragonal for 278 K < T < 395 K. The paraelectric BTO phase exists at higher temperature. With tetragonal BTO, $a = b = 0.399$ nm and $c = 0.403$ nm of P4mm space group. The spontaneous electric polarization of BTO lattice might be related with the displacement of the Ti^{4+} ion along the *c*-axis which is sensitive to the charge in hybridization of the 3d states of the Ti cation with the 2p states of the surrounding O anions. For single-phase $BaTiO_3$ with doping of transition metal ions, the Fe-doping into BTO is widely reported due to excellent magnetic behavior that originated from unpaired spin of Fe^{3+} ions [37]. However, the multiferroic nanocomposites may selected from perovskites such as $BaTiO_3$, $PbTiO_3$ and $BiFeO_3$ (due to their large polarization and piezoelectric coefficients) with ferrites which have high magnetostriction value, high resistivity, T_N above room temperature and large ferromagnetism [38].

2.2.1 Multi-layered heteroepitaxial multiferroic thin films

The ME coupling in composite phases is effectively tuned through interfacial strain, exchange-bias, field effects, and so on [39]. It is a way to construct film geometry on the basis of their dimensions. For example, a 0–3 configuration means that there are two phases in the composite, one consisting of zero-dimension particulates, and the other is three-dimensional bulk. However, the ME composites for film-on-substrate, the multi-layered epitaxial thin films (2–2 configuration) were firstly reported that to be results into strong ME coupling with higher quality of crystallography and intimate coherent interface. But the clamping effect of the substrate onto the ferroelectric (FE) phase reduces the magnitude of the ME coupling coefficient in thin films. For 1–3 configuration, *i.e.* the vertical nanostructures from perovskite and spinel systems, like $CoFe_2O_4$ nanopillars embedded in a $BaTiO_3$ or $BiFeO_3$ matrix, the substantial enhancement of ME coupling and electric-field

Synthesis method	Chemical composition; reaction time; precursor salts	Brief synthesis procedure & heating conditions of processing	Substrate; grain size (x); film thickness (d)
Sol–gel & spin coating [13]	**$BiFeO_3$:Ti, Sm, Nd**; **H**ours; $BiC_6H_5O_7$, $FeC_6H_5O_7.H_2O$, Sm_2O_3, Nd_2O_3, $Ti(iOPr)_4$, NH_3, C_2H_7NO, $C_6H_8O_7$, H_2O_2	Fe(III) and Bi(III) aqueous solution prepared by required amount of metal citrates in water. Fe(III) solution kept at 80°C with pH below 1.5 and added ammonia and ethanolamine into Bi(III) to increase the solution stability. The Sm & Nd salts mixed in citric acid & water and refluxed overnight at 120°C to get solid citrate and add NH_3 while refluxing at 110°C/2 h. The Ti(IV) aqueous prepared by hydrolyzing Ti (IV)-isopropoxide to precipitate the Ti(IV) hydroxide and the addition of a mixture of citric acid and hydrogen peroxide with heating at 60°C dissolves the precipitated hydroxide. Final solution dissolved with controlling pH and spin coated 3000 rpm/30s onto Pt(111)Ti/SiO_2/Si substrate and annealed at 600°C/ 1 h.	Pt(111)Ti/SiO_2/Si; $x < 100$ nm; $d \sim 250$ nm
Atomic layer deposition (**ALD**) [14]	**$BiFeO_3$**; **H**ours; tris(2,3-dimethyl-2-butoxy)bismuth(III), iron (III) tert-butoxide	Thin films of Bi-Fe-O and individual BiO_x and FeO_x grown by ALD on Pt/SiO_2/Si wafers using a commercial ALD reactor and precursors heated to 135–145°C providing enough vapor pressure for the deposition. The ozone (O_3) used as an oxidizing agent. The pulse duration for Bi $(mmp)_3$ and for ferrocene each <1 s and for ozone 5 s. The transport precursors kept at 150°C. The substrate placed ~3 cm from the gas inlet and the chamber heated to 250° C, and the gas outlet line kept at 100–150°C.	Pt/SiO_2/Si; $x = 30$ nm; $d = 50$ nm
Chemical spray [15]	**$BiFeO_3$:W**; **H**ours; $Bi(NO_3)_3{\cdot}5H_2O$, Fe $(NO_3)_3{\cdot}9H_2O$, $C_6H_8O_7$, Na_2WO_4	The Bi, Fe salts & 0.2 M citric acid dissolved in distilled water (added nitric acid to dissolve $Bi(NO_3)_3{\cdot}5H_2O$ and a 15 ml solution ready for spray. Second, 0.2 M $Na_2WO_4{\cdot}2H_2O$ added into a previous solution. These solutions sprayed separately onto non-conducting glass substrates at 400°C and the deposited films annealed at 500°C/ 4 h.	Non conducting glass; $x \sim 100$ nm; $d = 1$ μm
Chemical solution deposition using hydrothermal process [16]	**$BiFeO_3$**; **D**ays; $Bi(NO_3)_3{\cdot}5H_2O$, Fe $(CH_3COCHCOCH_3)_3$, $C_2H_4O_2$, $C_3H_8O_2$, Bi $(NO_3)_3{\cdot}5H_2O$, Fe $(NO_3)_3{\cdot}9H_2O$, KNO_3, PVA, KOH	BFO nanopowders as seeds prepared by hydrothermal method. 0.005 M $Bi(NO_3)_3{\cdot}5H_2O$ and 0.005 M Fe $(NO_3)_3{\cdot}9H_2O$ dissolved in 100 ml of diluted HNO_3 (10%) and 12 M KOH solution slowly added to the above solution to adjust pH ~8. The precipitates filtered and washed and mixed with 30 ml KOH (12 M) and 15 ml PVA (4 g/l). The suspension	Flexible polyimide; $x \sim 70$ (seeded) and ~ 100 nm (seeded + UV BFO); $d \sim 200$ nm

Synthesis method	**Chemical composition; reaction time; precursor salts**	**Brief synthesis procedure & heating conditions of processing**	**Substrate; grain size (x); film thickness (d)**
		solution transferred into Teflon lined stainless-steel autoclaves and kept at 160°C/9 h. The obtained BFO powders dispersed (using ultrasonic processor) in acetic acid and 1,3-propanediol. The seeded photosensitive BFO precursors used direct fabrication of BFO films onto a polyimide substrate under UV irradiation to get crystallized.	
Aerosol Assisted chemical vapor deposition [17, 18]	**$BiFeO_3$**; **D**ays; $[CpFe(CO)_2]_2$, $BiCl_3$, dichloromethane, THF	Aerosol assisted chemical vapor deposition (AACVD) uses a liquid–gas aerosol to transport soluble precursors to a heated substrate. A conventional atmospheric pressure CVD precursor proves in volatile or thermally unstable. For AACVD, the restrictions of volatility and thermal stability lifted the ionic precursors and metal oxide clusters used in aerosol assisted depositions. The AACVD reactions carried out using an in-house built coldwall CVD and annealed at 300°C	SICO coated float glass; $x \sim 100$ nm; d = 320–1700 nm
Metal–organic precursor complex solution [19]	**$BiFeO_3$**; **H**ours; $FeCl_3$, BCl_3, thiourea, methanol	The precursor solution prepared from ferric trichloride (0.1 M), bismuth trichloride (0.1 M), and thiourea (0.3 M, as an organic ligand) dissolved in methanol. The precursor complex is spin-coated onto the cleaned substrates at 1200 rpm and preheated at 473 K/10 min and annealed at 673 K/2 h.	Soda lime glass; $x \sim 150$ nm; d = 500 nm
Sol-electro-phoretic deposition [20]	**$BiFeO_3$**; **H**ours; $Bi(NO_3)_3{\cdot}5H_2O$, $Fe(NO_3)_3{\cdot}9H_2O$, 2-methoxy ethanol, citric acid, ethylene glycol	The solution prepared by dissolving $Bi(NO_3)_3{\cdot}5H_2O$ and $Fe(NO_3){\cdot}9H_2O$ in 2-methoxy ethanol. The citric acid and ethylene glycol added as complexing agents. The mixture sonicated for 10 min at room temperature until to gain a clear red sol suspension. The stainless steel mesh as working electrode and stainless steel (same dimension) as counter electrode and this substrate polished with emerged paper in oxalic acid and cleaned by acetone/ethanol. The EPD process for BFO film fabrication performed in red sol solution at 12 V within 60 s and the film crystalized at 500°C/2 h.	Stainless steel mesh; x = 100–150 nm d = 196 nm
Sol–gel: Evaporation-induced self-assembly (using **Dip** Coating) [21]	**$BiFeO_3$**; **D**ays; $Fe(NO_3)_3$, $Bi(NO_3)_3{\cdot}5H_2O$, 2-methoxyethanol, ethanol, glacial acetic acid	PB51-b-PEO62 block-copolymer with MW_{PB} = 51 000 g mol^{-1} and MW_{PEO} = 62 000 g mol^{-1} are polymer source as structure-directing agent. For solution A, PB51-b-PEO62 block-copolymer	$Pt/TiO_2/SiO_2/Si$; **Nanopores** (pore size = 100 nm); d = 66 nm

Synthesis method	Chemical composition; reaction time; precursor salts	Brief synthesis procedure & heating conditions of processing	Substrate; grain size (x); film thickness (d)
		dissolved in ethanol and 2-methoxyethanol at 70°C. Solution B prepared by dissolution of iron(III) nitrate and bismuth(III) nitrate in a mixture of 2-methoxyethanol, ethanol and glacial acetic acid. Solution B added to solution A to form the final solution. Nanopatterned porous and dense $BiFeO_3$ thin films deposited by dip-coating on $Pt/TiO_2/SiO_2/Si$ at 90°C and heated at 300°C/20 h, and annealed at 500°/10 min	
Hydro-thermal followed pulsed laser deposition [22]	**$BiFeO_3$**; **H**ours; $Bi(NO_3)_3.5H_2O$, $FeCl_3.6H_2O$, KOH	In hydrothermal process, 0.61 mM bismith nitrate and 0.55 mM iron chloride mixed with 100 mL of distilled water, and 0.9 M of KOH added as a mineralizer. The solution transferred to a 25-mL Teflon-lined autoclave and SRO/STO substrate positioned face down and placed ~1 cm above the bottom of the Teflon liner using Pt wire. A 10-nm-thick SRO layer deposited onto a STO substrate as the bottom electrode using pulsed laser deposition (PLD). The thin films deposited using a 4ω Nd:YAG laser (266 nm, 5 Hz repetition rate), the laser beam on ceramic targets kept to ~1.5 J/cm^2. The hydrothermal reaction taken at 200°C/6 h.	$SrRuO_3/SrTiO_3$; $x \sim 30$ nm d = 60 nm
Lithographic technique [23]	**0.65 BFO-0.35CFO**; **H**ours	Target material of BFO-CFO is prepared by any of the chemical method. BFO-CFO self-assembled nanostructures prepared by pulsed laser deposition using a 248 nm KrF laser. Growth carried out at 700°C in an oxygen atmosphere (150 mTorr) with a laser energy density of 3 J/cm^2 at 10 Hz. Etching of the annealed BFO-CFO performed in dilute HCl (50%, v/v) for 1 h at room temperature.	$SrTiO_3$; $x \sim 100$ nm; d = 500 nm
Solid state reaction - Pulsed laser deposition [24]	**$BiFeO_3$**; **D**ays; Bi_2O_3, Fe_2O_3, isopropyl alcohol	High-purity Bi_2O_3 and Fe_2O_3 powders weighed with 10 mol% excess Bi and thoroughly mixed by ball milling for 15 h using high-purity isopropyl alcohol and the mixture dried and calcined at 500–800°C/ 1.5 h. The leached residue of calcined powder pressed into pellets and sintered at 730°C/1 h. BFO thin films grown by PLD. A $SrRuO_3$ electrode having 50 nm thickness deposited on a $SrTiO_3$ (100) substrate at 600°C	$SrTiO_3$; $x \sim 150$–200 nm $d \sim 250$ nm

Synthesis method	Chemical composition; reaction time; precursor salts	Brief synthesis procedure & heating conditions of processing	Substrate; grain size (x); film thickness (d)
		in an oxygen ambient of 100 mTorr.	
Microwave assisted sol–gel & spin coating [25]	**$BiFeO_3$**; **D**ays; $Fe(NO_3)_3{\cdot}9H_2O$, $Bi(NO_3)_3{\cdot}5H_2O$, $(CH_2OH)_2$	Bismuth nitrate and Iron nitrate dissolved in ethylene glycol at room temperature separately and then mixed together. Resultant solution subjected to microwave radiations using microwaves operated at 2.45 GHz (microwave powers in 180–1000 W). The microwave assisted bismuth iron oxide solution spin coated on Cu substrates with using 3000 rpm/20s and then annealed in vacuum and 500 Oe field at 300°C/60 min.	Cu; x = 16–26 nm d = 700 nm
Non-aqueous sol–gel [26]	**$Bi_{0.9}Ho_{0.1}FeO_3/TiO_2$**; **D**ays; $Bi(NO_3)_3.5H_2O$, $Fe(NO_3)_3.9H_2O$, $Ho(NO_3)_3.5H_2O$, $C_6H_8O_7$, $C_2H_6O_2$, $Ti(O\text{-}nBu)_4$, n-BuOH, $C_5H_8O_2$, CH_3COOH	For 1 g $Bi_{0.9}Ho_{0.1}FeO_3/TiO_2$ (BHFO) powder, the stoichiometric proportion of $Bi(NO_3)_3.5H_2O$ (0.003 M), $Fe(NO_3)_3.9H_2O$ (0.0033 M), $Ho(NO_3)_3.5H_2O$ (0.00033 M), $C_6H_8O_7$ (0.0067 M) and $C_2H_6O_2$ (10 ml) dissolved in deionized water and the solution heated at 75–85°C/4 h to get gel which dried at 100°C/24 h and annealed at 500°C/2 h. For the preparation of BHFO nanoparticles/TiO_2 composite thin films, first n-BuOH (0.0884 M) and $C_5H_8O_2$ (0.0015 M) mixed and, then $Ti(O\text{-}nBu)_4$ (0.005 M) added to the solution. CH_3COOH (0.001 M) slowly added into the alkoxide solution and stirred. Thin films containing 5 mol.% BHFO ($T^{95}B^5$), 10 mol.% BHFO ($T^{90}B^{10}$) and 20 mol.% BHFO ($T^{80}B^{20}$) prepared using non aqueous sol–gel method. To synthesize composite films, molar amount of n-BuOH, $C_5H_8O_2$, $Ti(O\text{-}nBu)_4$ and CH_3COOH kept similar as that of pure thin film. Firstly 0.0442 M of n-BuOH taken and calculated amount of BHFO nanoparticles mixed into it for every composite film. The whole mixture dispersed vigorously in an ultrasonic bath and then $C_5H_8O_2$, $Ti(O\text{-}nBu)_4$ and rest of n-BuOH (0.0442 M) added into this mixture and then taken into ultrasonic bath in which CH_3COOH added dropwise. The solutions spin-coated onto the glass substrate at 2000 rpm/30s and annealed at 500°C/2 h.	Glass; $x \sim 60$ nm; d = 200 nm (TiO_2), 244 nm ($T^{95}B^5$), 477 nm ($T^{90}B^{10}$), 635 nm ($T^{80}B^{10}$)
Photosensitive sol–gel using	**$Bi_{0.85}La_{0.15}Fe_{0.95}Mn_{0.05}O_3$**; **D**ays; $Bi(NO_3)_3.5H_2O$, La	Benzoylacetone BzAcH preferred as the chelating agent and 2-methoxyethanol (MOE) as the	Si (100); $x \sim 50$ nm d = 140 nm

Synthesis method	Chemical composition; reaction time; precursor salts	Brief synthesis procedure & heating conditions of processing	Substrate; grain size (x); film thickness (d)
Dip coating [27]	$(NO_3)_3.6H_2O$, Mn $(NO_3)_2.4H_2O$, Fe $(NO_3)_3.5H_2O$, Benzoylacetone,	solvent. Four kinds of solutions of bismuth nitrate-BzAcH-MOE, lanthanum nitrate-BzAcH-MOE, manganese nitrate-BzAcH-MOE and ferric nitrate-BzAcH-MOE with the same molar ratio of nitrate: BzAcH:-MOE = 1:0.6:4 prepared beforehand. Therefore, the BLFMO solution obtained by mixing these four solutions with the total metallic ion concentration of 0.5 mol L^{-1}. The BLFMO gel film fabricated on Si (100) substrate by the dip-coating, and undergo irradiation and annealed at 650°C/1 h.	
Polymer assisted deposition from aqueous solutions [28]	**$BiFeO_3$**; **D**ays; $Bi(NO_3)_3.5H_2O$, Fe $(NO_3)_3.9H_2O$, ethylenediaminetetraacetic acid, polyethylenimine	Heteroepitaxial thin films of BFO (a_{BFO}^{pc} = 3.965 Å) deposited on cubic (001)STO (a_{STO} = 3.905 Å) by Polymer assisted deposition from aqueous-based solutions. Individual solutions of Bi^{3+} and Fe^{3+} prepared by dissolving their respective hydrated nitrates in deionized water with ethylene diamine tetra acetic acid (EDTA, 1:1 molar ratio) and polyethylenimine (PEI) (2:1 and 1:1 mass ratio to EDTA for Bi and Fe, respectively). The corresponding pH was 8.1 for Bi and 5.1 for Fe. Each single solution then filtrated and the retained portions analyzed by inductively coupled plasma atomic emission spectroscopy yield a final concentration of 79 and 200 mM for Bi and Fe, respectively. The filtrated solutions mixed according with final stoichiometry and concentrated to a final value 0.25–0.3 M, in order to obtain films in the range 25–30-nm-thick. 30 μL of final solution with Bi/Fe (1:1) was spin coated (4000 rpm/20 s) on (001)STO substrates and annealed in 600–900°C/3 h.	(001)STO; $x \sim 30$ nm d = 30–60 nm
Radical enhanced atomic layer deposition (**RE-ALD**) [29]	**$BiFeO_3$**; **D**ays; Tris(2,2,6,6-tetramethyl-3,5-heptanedionato) bismuth(III) [Bi $(TMHD)_3$], $Fe(TMHD)_3$	The deposition of metal oxide thin films used β-diketonate precursors and oxygen radicals. The multibeam system used in this study consists of a 10 in.-outer diameter stainless steel main chamber along with a load-lock assembly to facilitate sample insertion and removal without exposing the entire system to atmosphere. Pressure in the chamber maintained between 1×10^{-6} Torr at base and 2×10^{-5} Torr during operation by a CTI 4000 L/s cryogenic pump. The beams of the atom source and the precursor dosers	(001)$SrTiO_3$; x = 50–100 nm d = 93.5 nm

Synthesis method	Chemical composition; reaction time; precursor salts	Brief synthesis procedure & heating conditions of processing	Substrate; grain size (x); film thickness (d)
		converged onto a heated sample stage where the substrate mounted. Oxygen radicals produced from the atom source using a 2.46 GHz Sairem microwave power supply at 25 W and ~0.6 sccm O_2 gas. Depositions carried out from 190 to 230°C.	
RF magnetron sputtering [30]	**$BiFeO_3$-$CoFe_2O_4$**; **D**ays; Bi_2O_3, Fe_2O_3, Co_3O_4	BFO-CFO nanocomposite ceramic target prepared by a conventional oxide sintering method from Bi_2O_3 and Fe_2O_3. The final composite target prepared from BFO and CFO powders and mixed using ball milling for 24 hours then dried and pressed into a pellet and sintered at 800°C/5 h. The 2 inch diameter sintered target polished then bonded to a Cu plate using indium shot on a hot plate at 200°C. BFO-CFO nanocomposite films grown on (001)Nb-doped $SrTiO_3$ substrates. Deposition conducted at substrate temperatures of 480-650°C and working pressure 50 mTorr with Ar: oxygen ratios of 1:4 and 1:9. The chamber initially pumped to 5×10^{-6} Torr base pressure and the RF power 60 W.	Nb-doped $SrTiO_3$ (001); x = 20–25 nm d = 200 nm
Soft Chemical method and **Spin**-coating [31]	**$BiFeO_3$**; **H**ours; Iron(III) nitrate nonahydrate, Bismuth nitrate, ethylene glycol, citric acid	The precursor solutions of bismuth and iron were prepared by adding to the ethylene glycol and citric acid. The molar ratio of metal/citric acid/ethylene glycol was 1/4/16. The viscosity of the resulting solution adjusted to 20 cP by controlling the water content using a Brookfield viscosimeter. The films spin-coated from a BFO deposition solution onto $Pt/Ti/SiO_2/Si$ substrates and annealed at 500°C/2 h.	$Pt/Ti/SiO_2/Si$; x = 53–58 nm d = 200–300 nm
Three in one solution approach [32]	**$BiFeO_3$**; **D**ays; $Bi(NO_3)_3{\cdot}5H_2O$, $Fe(NO_3)_3{\cdot}9H_2O$, $CH_3N(CH_2CH_2OH)_2$, $HO(CH_2)_3OH$, CH_3CH_2OH,	Metal nitrates first dissolved at room temperature in a mixture of MDEA and 1,3-propanediol solvents using a molar ratio of 1:5:10 (metal:MDEA: diol) and the complexing reactions promoted by heating at 150–190°C/120 min. After diluting with ethanol, stable solutions of Bi-MDEA and Fe-MDEA precursors obtained with a concentration of 0.3 M. Stoichiometric amounts of these solutions mixed together to get $BiFeO_3$ (0.3 M). For $BiFeO_3$ film, layers from the respective precursor deposited on $Pt/TiO_2/SiO_2/(100)Si$ substrates by spin coating (2000 rpm/45 s) and dried on a hot	Flexible polymer substrates (polyimide); x = 55 nm; d = 185 nm

Synthesis method	Chemical composition; reaction time; precursor salts	Brief synthesis procedure & heating conditions of processing	Substrate; grain size (x); film thickness (d)
		plate at 150°C/5 min, and subjected to UV irradiation in oxygen at 150°C/ 30 min.	
Wet Chemical route [33]	**$BiFeO_3$**; **H**ours; $Bi(NO_3)_3$. $5H_2O$, $Fe(NO_3)_3$. $9H_2O$, ammonium hydroxide, ethanol, acetic acid, diethanolamine, 2-ethoxyethanol	In the first step, an aqueous solution of ferric nitrate treated with ammonium hydroxide (25%) solution and the precipitate washed with distilled water. 4 mL of acetic acid (95%) then added into it under stirring and heated at 75°C/30 min, and five drops (0.00419 M) of diethanolamine (DEA) added. In the second step, a required amount of bismuth nitrate dissolved in 20 mL 2-ethoxyethanol solvent and then 0.5 mL acetic acid (95%) also added into it and also added five drops (0.00419 M) of DEA. Both the solution mixed together and the precursor deposited by dip coating (speed 6 cm/min) and spin coating process (4000 rpm for 20 s) on ITO substrates.	ITO; x = 5 nm; d = ∼ 2 μm and ∼ 200 nm
Laser molecular-beam epitaxy [34]	**$BiFeO_3$**; **H**ours	Epitaxial BFO thin films of various thicknesses of 2, 4, 8, 19, 38, 57, 94, 141, 188, 283, and 449 nm were deposited on (001)-oriented STO and slightly Nb-doped STO single crystals by a laser molecular-beam epitaxy system. The films deposited at 560°C using an excimer XeCl laser (1.5 J/cm^2, 308 nm, 2 Hz) at oxygen pressure of 2 Pa (2×10^{-2} mbar). After deposition, the films subjected into situ annealed for 30 min then cooled down slowly to room temperature [35].	(001)-oriented STO; x = 8 nm d = 8–449 nm

Bold emphasis has more significance.

Table 1.
Synthesis methods used to prepare multiferroic $BiFeO_3$ (BFO) thin films.

induced magnetization switching observed. It is due to the effect of large heteroepitaxial interface and reduced clamping effect. In **Figure 4a**, the new structure that fully epitaxial multilayered nanodot array, *i.e.* 0–0 composite which combines the advantages of 2–2 and 1–3 geometries to obtain a better understanding of extrinsic ME coupling and build prototypes for high density multistate memory devices. In 2–2 type, the horizontal stacking, *i.e.* an epitaxial multilayer or superlattice can provide more flexibility for material design, composition control, and layer arrangement.

2.2.2 SEM images of $BaTiO_3$-$CoFe_2O_4$ (BTO-CFO) two-layered nanodots

A typical scanning electron microscope (SEM) image of the as obtained STO/ AAO substrate is given in **Figure 4b** [39]. There is no gap found between STO and

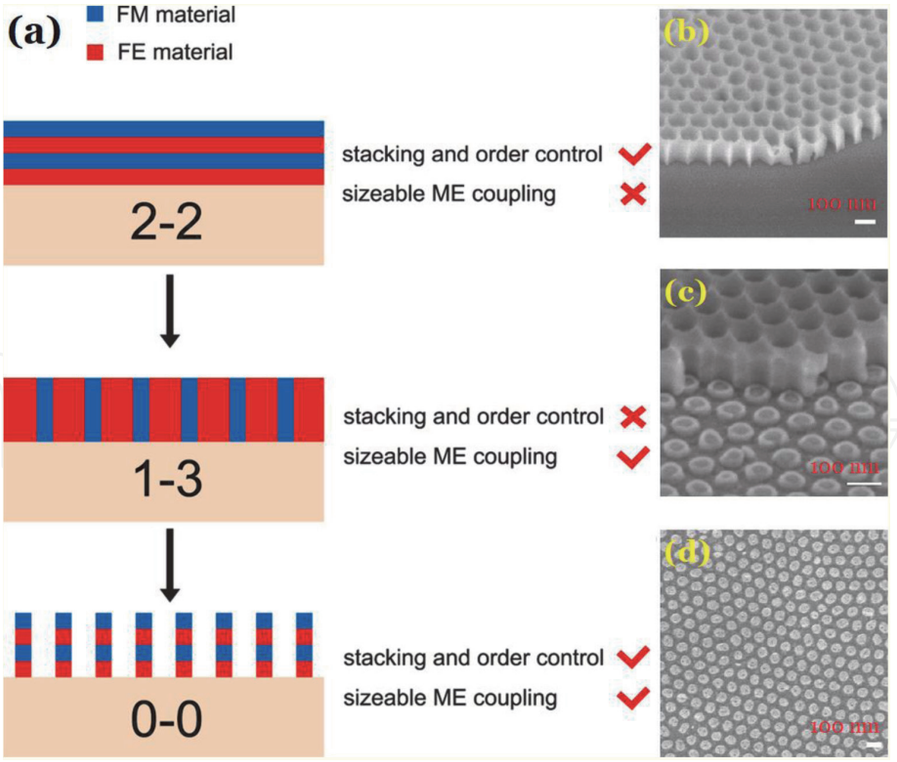

Figure 4.
(a) The film-on-substrate geometry in ME composites. SEM images of (b) as-transferred anodic aluminum oxide (AAO) mask on STO substrate, (c) BTO nanodots with partly removed AAO in first layer deposition, (d) BTO/CFO two-layered nanodot arrays [39].

the AAO membrane (thickness ~ 120 nm and pore diameters ~65 nm). The thin films are synthesized by PLD process. In **Figure 4c** and **d**, the highly ordered nanodot arrays with flat surfaces and diameters around 65 nm were obtained. The AAO was fabricated through a self-assembly process, the periodic area is only μm^2 in size.

2.2.3 Synthesis techniques for $BaTiO_3$ thin films

The thin film processing issues associated with various techniques such as the formation of side phases and the difficulty in controlling stoichiometry, film thickness, and sample crystallinity. For this we have summarized some synthesis method for $BaTiO_3$ based multiferroic thin films described in **Table 2**.

2.3 $PbTiO_3$ multiferroics

Since ferroelectricity in perovskites ABO_3 commonly involves B-site transition-metal ions with a formal electron configuration d^0 (e.g. Ti^{4+}, Nb^{5+}, etc.), while magnetism requires TM cations with partially filled d states. A lot of studies on multiferroics concentrate on the Bi-based perovskites, *i.e.* $BiFeO_3$ and $BiMnO_3$, where the ferroelectricity mainly arises from the lone pair of 6 s electrons [53]. But the basic physics in the ferroelectric thin films is similar to the bulk state in addition to some specific properties in thin-film like interface strain and stress, dead layer effect etc. [54]. In perovskites, $PbTiO_3$ also have multiferroic behavior with TM doping or composites substitution and have spontaneous polarization parallel to the *c* axis. The lattice structure of $PbTiO_3$ is tetragonal below the T_C and turns into cubic and paraelectric above T_C. The value of T_C for bulk $PbTiO_3$ lies in 490–493°C which depends upon synthesis process, size or defect effect. The displacement of the Ti

Synthesis method	**Chemical composition; reaction time; precursor salts**	**Brief synthesis procedure & heating conditions of processing**	**Substrate; grain size (x); film thickness (d)**
Atomic oxygen assisted molecular beam epitaxy (**AO-MBE**) [40]	**$BaTiO_3/CoFe_2O_4$**; **H**ours; Metallic individual Ba, Ti, Co, Fe	Films deposited by evaporation of metallic individual Ba, Ti, Co, Fe from dedicated Knudsen cells assisted by a high brilliance (350 W- 10^{-7} mbar oxygen -baratron 3.1 tr) atomic oxygen plasma with growth rate ~ 0.5-2 Å/min. Metal Ba kept in oil before insertion in the chamber because of its high reactivity with water and the oil removed using C_6H_{12} ultrasound assisted baths. The wet Ba metal introduced in MBE system just prior pumping, the procedure allows easy and fast outgassing of the Ba charge. This approach has advantage of enabling independent Ti, Ba, Co, Fe dosing as well as oxygen dosing.	Nb:$SrTiO_3$ (001) and Pt (001); $x < 25$ nm; $d \sim 30$ nm
Chemical bath deposition [41]	**$BaTiO_3$**; **H**ours; $Ba(CH_3COO)_2$, Ti (C_4H_9O), acetic acid, ethylene glycol, butanol	In chemical bath deposition, the substrate is immersed in a solution containing the precursors which depends upon parameters like bath temperature, pH of the solution, the molarity of concentration, and time. Two solutions of barium acetate in butanol and acetic acid, and tetra-butyl titanate in butanol and ethylene glycol are mixed to get a final product. Thin films of $BaTiO_3$ grown on glass substrates with solution temperature 78° C and annealed at 300°C/1 h.	Glass; x = 23–30 nm
Chemical solution deposition [42]	**$BaTiO_3$-$CoFe_2O_4$**; **H**ours; $Ba(CH_3COO)_2$, $(C_4H_9O)_4Ti$, Fe $(NO_3)_3.9H_2O$, Co $(CH_3COO)_2$. $24H_2O$, 2-methoxyethanol, acetic acid, ethanolamine	2-Methoxyethanol and acetic acid used as the solvents with a ratio of 3:2 in volume for preparing both BTO and CFO precursors. Ethanolamine added to adjust the viscosity. The films spin-coated on Pt/Ti/SiO_2/Si(100) substrate with 6000 rpm/10s. The BTO precursor deposited on the substrate firstly, and baked in a 350°C preheated tube furnace for 10 min in air after each coating and pre-sintered for 10 min/700°C. After that the CFO layer deposited on the BTO layer, finally, the film annealed for 700° C/2 h.	Pt/Ti/SiO_2/Si (100); $x \sim 11$ nm; d = 500 m
Solid state reaction and DC sputtering [43]	**$La_{0.7}Ca_{0.3}MnO_3$/ $BaTiO_3$**; **D**ays; Oxides of La, Ca, Mn, Ba, Ti	The base material is prepared by a solid state or any chemical synthesis method. Films were grown on [001] oriented BTO and [100] oriented STO single crystal substrates at high O_2 pressure dc sputtering at 900°C.	$BaTiO_3$; x = 300 nm
Electrophoretic Deposition [44]	**$BaTiO_3/CoFe_2O_4$**; **D**ays; Acetates of Ba, Fe, Co, $Ti(C_4H_9)O_4$, ethanol, acetic acid, NaOH,	$BaTiO_3$ and $CoFe_2O_4$ powders were prepared using **sol–gel** and **chemical co-precipitation** method, respectively. Tween 80 and polyethylene imine polymers used as dispersants, and polytetra fluoro ethylene made	Al_2O_3/Pt; $x \sim 100$ nm; $d \sim 50$ μm

Synthesis method	Chemical composition; reaction time; precursor salts	Brief synthesis procedure & heating conditions of processing	Substrate; grain size (x); film thickness (d)
	Tween 80, polyethylene imine	rectangular cell used as the electrophoresis tank for the electrophoretic deposition where Al_2O_3/Pt acted as cathode for film deposition. The deposited films sintered at 600 and 1200°C	
Liquid phase deposition [45]	**5–50 wt % $CoFe_2O_4$-$BaTiO_3$; D**ay; Barium, titanium(IV) isopropoxide, cobalt and iron acetylacetonate, anhydrous benzyl alcohol, acetone, 2-propanol, methoxyethoxy) ethoxy] acetic acid, and hexane, ethanol	For the synthesis of $BaTiO_3$ nanoparticles, 137 mg of dendritic Ba dissolved in 5 mL of degassed acetophenone at 80°C in an argon filled glovebox, with dropwise addition of a titanium isopropoxide and the mixture transferred to a microwave vial, sealed, and exposed to microwave irradiation at 220°C/30 min. For $CoFe_2O_4$ synthesis, 353 mg of $Fe(C_5H_7O_2)_3$ and 120 mg of Co $(C_5H_7O_2)_2$ mixed with 5 mL of benzyl alcohol in an argon-filled glovebox and subjected to microwave irradiation at 180°C/30 min in a 10 mL Teflon-capped glass vessel. The $BaTiO_3$ and $CoFe_2O_4$ nanoparticles are centrifuged off at 4000 rpm, washed with ethanol, and finally sonicated for 45 min in 0.3 M ethanolic MEEAA solution using a ultrasonic cleaner. In the next step, an excessive amount of hexane (5:1 hexane to ethanol ratio) is added, and the mixture is centrifuged to separate the nanoparticles. Afterward, the $BaTiO_3$ and $CoFe_2O_4$ nanoparticles redispersed in ethanol with sonication. The co-dispersions $BaTiO_3/CoFe_2O_4$ mixure deposited using spin-coating (1000 rpms/20s) and heated at 500°C and film annealed at 700°C/2 h.	$Pt/TiO_2/SiO_2/Si$; x = 13 nm; d = 400–500 nm
Sol–gel followed magnetron sputtering [13, 46]	**$BaTiO_3$-$Ni_{0.5}Zn_{0.5}Fe_2O_4$; H**ours	The BTO and NZFO synthesized via sol gel and citric acid combustion method and sintered at 1200°C/2 h. The sputtering atmosphere was set at 0.4 O_2 and 0.6 Ar_2 with a total pressure of 0.6×10^{-3} bar, and the sputtering power adjusted between 80 W and 250 W (sputtering time selected between 2 and 6 h). The deposited films annealed at 600 -820°C.	(100) and (111) Si; $x \sim 20$ nm; $d \sim 100$ nm
Metallo-organic decompositi (**MOD**) [38]	**$MFe_2O4/BaTiO_3$; D**ays; xylene, 2-ethylhexanoic acid, KOH, Ba, Fe, Mn, Co, Ni, Zn nitrates, $C_{16}H_{36}O_4Ti$, polyethylene glycol, acetone, isopropanol	0.1 M solution of 2-ethylhexanoic acid was neutralized with KOH and then mixed with respective nitrates of Ba, Mn,Co, Ni and Zn. Each film was taken in 1:1 ratio. Final solution was refluxed at 110°C/10 h and then PEG used as binder in the coating MFO/BFO solution. The solution coated on $Pt/Ti/SiO_2/Si$ substrate using spin-coating (4500 rpm/60 s) and annealed at 600°C/3 h.	$Pt/Ti/SiO_2/Si$; x = 20–137 nm; $d \sim 600$ nm

Synthesis method	Chemical composition; reaction time; precursor salts	Brief synthesis procedure & heating conditions of processing	Substrate; grain size (x); film thickness (d)
Off-axis RF magnetron sputtering [47]	**$BaTiO_3$-$BiFeO_3$**; **H**ours	Buffered oxide etchant (BOE) used to treat the surface of STO substrate followed by annealing at 900°C in an O_2 atmosphere. LSMO thin film deposited on STO substrate at 600°C at 5 m Torr with 8:2 O_2:Ar gas ratio and 4.93 W cm^{-2} of RF power. $BaTiO_3$-$BiFeO_3$ thin film grown on the epitaxial LSMO thin film at 400°C via in-situ deposition under same RF power and pressure with 1:9 O_2:Ar gas ratio.	$SrTiO_3$; x = 200–500 nm; d = 80–500 nm
Polymer-assisted deposition [48]	**$BaTiO_3$-$CoFe_2O_4$**; **H**ours; EDTA, PEI, Ba, Fe, Co, Ti chlorides,	Barium chloride or iron chloride added to the solution of an ethylenediammine tetraacetic acid (EDTA) and Polyethylenimine (PEI). Cobalt chloride added to PEI solution at pH -7, and the mixture of titanium chloride and peroxide added to the mixture of PEI and EDTA to maintain pH 7.5. All the solutions mixed with a molar ratio of Ba: Ti:Co:Fe = 1:1:1:2 followed by spin coating on LAO substrates at 2000 rpm/ 30s and the samples heated at 500°C and annealed at 900°C/1 h.	$LaAlO_3$ (100); $x \sim$ 90 nm; $d \sim$ 100 nm
One-step Pulsed laser deposition followed Solid State Reaction [49]	**$(BaTiO_3)_{0.8}$: $(La_{0.7}Sr_{0.3}MnO_3)_{0.2}$**; **D**ays; $BaTiO_3$, La_2O_3, $SrCO_3$, MnO_2	Solid state sintering method used to synthesize target sample BTO:LSMO with atomic ratio 8:2. The STO (001) substrates used to deposit thin films via pulsed laser deposition. The temperature of 750°C in a 200 mTorr oxygen atmosphere was maintained during deposition and a 400 mJ laser was used to shot the targets for 3000 pulses. The substrate distances kept at 4.5 cm, and cooling of the films in 200 mTorr oxygen atmosphere to room temperature was done after deposition.	STO (001) x = nanopillars; d = 90–117 nm
Laser molecular beam epitaxy [50]	**$(Bi_{0.5}Na_{0.5})TiO_3$-$BaTiO_3$** (**Mn** doping); **H**ours; Oxides of Bi, Na, Ti, Ba, Mn	Conventional sintering method used to synthesize Mn doped BNBTMn by using excess of Bi_2O_3 thin layer of $La_{2/3}Sr_{1/3}MnO_3$ deposited on STO substrate at 800°C. The films grown on LSMO coated STO substrate at 750°C by deposition of LSMO dot top electrodes through a shadow mask on the surface of BNBTMn at 700°C. The laser with power of 5 J/cm^2 and oxygen partial pressure of 200 mTorr was used for all depositions.	(001)STO; $d \sim$ 400 nm
Two-step anodization process followed spin-coating [51]	**$BaTiO_3$-$CoFe_2O_3$**; **H**ours; Ti foil, NH_4F, ethylene glycol, dimethyl sulfoxide, $Ba(OH)_2$, $Co(CH_3COO)_2{\cdot}4H_2O$, $Fe(NO_3)_3{\cdot}9H_2O$, 2-methoxyethanol	Two step anodization process was used to prepare TNTs. First step included anodization of Ti foil in an ethylene glycol-based electrolyte containing 0.09 M NH_4F and 1.24 M H_2O at 60 V. Second step included the use of mixture of ethylene glycol and dimethyl sulfoxide containing 0.1 M NH_4F and	Ti substrate; $x \sim$ nanopillars (diameter 40–50 nm, length 2600 nm)

Synthesis method	Chemical composition; reaction time; precursor salts	Brief synthesis procedure & heating conditions of processing	Substrate; grain size (***x***); film thickness (***d***)
		1.5 M H_2O at 60 V, 60°C/min followed by 15 minute treatment with electrolyte. TNTs were then treated with $Ba(OH)_2$ aqueous solution in a Teflon lined hydrothermal reactor at 180°C/2 h. CFO precursors were prepared by mixing Co $(CH_3COO)_2.4H_2O$ and $Fe(NO_3).9H_2O$ in 2-methoxy ethanol and H_2O followed by ultrasonication for 1 h. The spin coating of BTO with CFO was done to prepare BTO/CFO nanocomposite at 4000 rpm and 260°C/10 min. Final sample calcined at 600°C/3 h	
Tape casting method [52]	**Fe_3O_4@$BaTiO_3$/P (VDF-HFP)**; **D**ays; $FeCl_3$, CH_3COOK, EG, $C_4H_{10}O$, $C_{19}H_{42}BrN$, $C_{16}H_{36}O_4Ti$, $Ba(OH)_2$, CH_3COOH, N, N-C_3H_7NO, P(VDF-HFP)	The FO submicron spheres prepared by a solvothermal synthesis and the FO@BTO core-shell particles prepared by a two-step hydrolysis-hydrothermal method. The required amount of core-shell FO@BTO powder dispersed in 10 ml DMF and placed in an ultrasound bath for 4 h. Then a calculated amount of P(VDF-HFP) dissolved into the suspension using an ultrasonic bath with stirring. The films of P(VDF-HFP) and core-shell particles prepared by tape casting and dried at 80°C and heated at 200°C/7 min and quenched in ice water immediately.	***x*** = 352 nm (FO), 8 nm (BTO); ***d*** = 15 μm

Bold emphasis has more significance.

Table 2.
Synthesis method used to process $BaTiO_3$ based multiferroic thin films.

atom in the O octahedron gives the spontaneous polarization of the $PbTiO_3$ due to the vector of polarization from the center of the O octahedron to the Ti atom. Through the substitutions for Pb or Ti or both cations, the ferroelectric properties could be widely modified and the structures could show various characters. Due to scarcity of multiferroics, $PbTiO_3$ is being extensively studied for induction of magnetism. The large 'Pb' cation is coordinated by twelve oxygens in a cub-octahedral way, while the smaller 'Ti' cation is octahedrally coordinated with six oxygens [55]. The large degree of ferroelectricity in $PbTiO_3$ occurs to the contribution of covalent bonds between both Pb 6p - O 2p and Ti 3d - O 2p states. The covalent bond between Pb 6p and O 2p lowers the non-centrosymmetric symmetry towards the ferroelectric state by weakening the ionic core repulsion between Pb and the nearest oxygen ions.

2.3.1 ME coupling due to ferroelectric polarization under an external magnetic field

Figure 5a shows spontaneous polarization (P-E loop) under the influence of a magnetic field (H = 0–0.5 T) for $Pb_{0.7}Sr_{0.3}(Fe_{0.012}Ti_{0.988})O_3$ thin film. This thin film prepared by a MOD method and deposited on $Pt/Ti/SiO_2/Si$ substrate using spin-coating [56]. The magnetic switching from $+P_r$ to zero at 0.5 T have been observed.

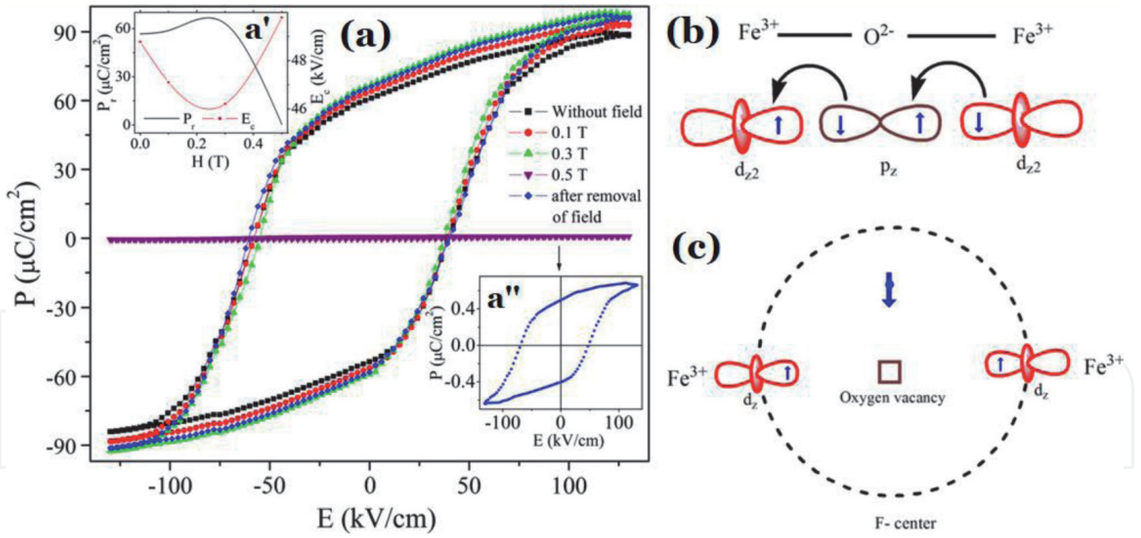

Figure 5.
(a) Ferroelectric hysteresis under an external magnetic field (0–0.5 T) for $Pb_{0.7}Sr_{0.3}(Fe_{0.012}Ti_{0.988})O_3$ thin film. (a′) Variation of P_r and E_c with applied H. (a) P ~ 0 at 0.5 T (contribution by electrode) [56]. (b and c) F-center exchange mechanism responsible for room-temperature ferromagnetism in Fe-doped $PbTiO_3$ [57].

In **Figure 5a′**, the polarization is continuously increased with increasing H up to 0.3 T which is an indication for the coupling between the polarization and magnetization. When a magnetic field applied to a ME material, the material is strained to induce a stress on the piezoelectrics to generates the electric field. This field related with ferroelectric domains resulting into an increase in polarization. **Figure 5a″** shows a low polarization response with lossy hysteresis at 0.5 T, which may have been caused by the electrode.

2.3.2 Mechanism for ferromagnetism in Fe-doped $PbTiO_3$

F-center exchange (FCE) mechanism is used to evaluate the magnetic origin in $Pb(Ti_{1-x}Fe_x)O_3$ thin films as shown in **Figure 5b** and **c** [54, 57]. As the tetravalent Ti^{4+} is replaced by trivalent Fe^{3+} cations, there is generation of oxygen vacancies to cause charge neutrality in the multiferroic. An electron trapped in the oxygen vacancy might to produce an F center, where the electron occupies an orbital to overlaps the *d* shells of both iron neighbors. As the unoccupied spin orbitals are minority in the $3d^5$ of Fe^{3+}, the trapped electron and the iron neighbors have opposite spin direction. Therefore, the system becomes ferromagnetic due to super-exchange effect generates antiferromagnetism.

2.3.3 Synthesis techniques for $PbTiO_3$ thin films

To the investigation of bulk ferroelectric materials, the compositional adjustment has plays a major role to study new ferroelectric. However for thin films, the suitability of synthesis method for processing of epitaxial ferroelectric plays key feature to change the polarization behavior due to some technical features related with film geometry on substrate. In **Table 3**, we have introduced some typical synthesis routes for $PbTiO_3$-based multiferroic thin films fabrication.

2.4 Multiferroic $CaTiO_3$ systems

Since $CaTiO_3$ (CTO) is prototype for the perovskite structure [67]. At room temperature, CTO has the orthorhombic $GdFeO_3$ type crystal structure (*a* = 5.38 Å,

Synthesis method	Chemical composition; reaction time; precursor salts	Brief synthesis procedure & heating conditions of processing	Substrate; grain size (x); film thickness (d)
Chemical solution deposition [58]	**$0.7BiFeO_3$–$0.3PbTiO_3$** (**Mn** doping); **D**ays; $Bi(O^tC_5H_{11})_3$, Fe $(OC_2H_5)_3$, Pb $(CH_3COO)_2$, Ti $(O^iC_3H_7)_4$, Mn $(O^iC_3H_7)_2$, 2-Methoxyethanol	Calculated amounts of $Bi(O^tC_5H_{11})_3$, Fe $(OC_2H_5)_3$, $Pb(CH_3COO)_2$, $Ti(O^iC_3H_7)_4$ and $Mn(O^iC_3H_7)_2$ were dissolved in 2-Methoxyethanol which acted as solvent. The Mn content set at 5 mol% for Fe site, solution refluxed for 20 h, and the entire process conducted in dry N_2 environment. Thin films were fabricated via spin coating at 2500 rpm/30s on $Pt/TiO_x/SiO_2/Si$ substrates followed by drying at 150°C/5 min and calcined at 400°C/1 h in O_2 flow.	$Pt/TiO_x/SiO_2/Si$; $x \sim 60$ nm; $d \sim 500$ nm
DC magnetron sputtering [59]	**$(Co/Ni)_4/Pb(Mg_{1/3}Nb_{2/3})O_3$-$PbTiO_3$**; **D**ays	Multi-layered multiferroic films grown on a (001)-cut single crystal PMN-PT substrate at pressure below 7×10^{-6} (5×10^{-8} Torr), and Ar^+ ion bombarded to remove organic contamination. The various multilayered films with different thickness where 3 nm Ta adhesion layer was followed by 2 nm Pt to encourage (111) face-centered-cubic growth of subsequent film. Ni thickness was altered between 0.15 and 0.9 nm to synthesize five Co/Ni multi-layered films PMN-Pt: [Co (0.6 nm)/$Ni(tNi]_{x4}$/Co (0.6). The capping layers were identical initiating with a 2 nm Pt layer with a protective 3 nm Ta capping electrode. A fixed power of 40 W and a pressure of 0.7 Pa are used.	[001]-cut PMN-PT; d = ultrathin
Hydrothermal method [60]	**$LaFeO_3$-$PbTiO_3$**; **D**ays; $Pb(NO_3)_2$, La $(NO_3)_3.6H_2O$, Fe $(NO_3)_3.9H_2O$, TiO_2, KOH	$Pb(NO_3)_2$, $La(NO_3)_3.6H_2O$, Fe $(NO_3)_3.9H_2O$ and TiO_2 were thoroughly mixed in 9 M solution of KOH, and mixture stirred for 2 h and then transferred to Teflon-lined stainless autoclave having a single crystal (001) oriented NSTO at the bottom of the autoclave. The sealed autoclave heated at 200°C/36 h	**Nb-$SrTiO_3$ (100)**; $x \sim 20$ nm; $d \sim 250$ nm
Laser ablation [61]	**$PbTiO_3$-$CoFe_2O_4$**; **H**ours	Pure PTO and CFO target were prepared by any of chemical synthesis method. $PbTiO_3$-$CoFe_2O_4$ thin films formed by depositing $CoFe_2O_4$ and $PbTiO_3$ via laser ablation in the superlattice spread. The average composition changes continuously from one end (pure PTO) to the other (pure CFO) films deposited on MgO substrate at 600°C and oxygen partial pressure of 65 mTorr. The energy used for ablation was ~2 J/cm^2. The total thickness at each position on the spread was 300 nm, and sample ~ 6 mm long in the direction of spread.	(100) MgO; $x \sim 30$ nm; $d \sim 12.6$
Metal–organic chemical vapor	**$CoFe_2O_4$-$PbTiO_3$**; **H**ours; Co tris(2,2,6,6-	The c-axis orientation chosen for substrate, and the procedure included evaporation of metal organic precursors	(001) $SrTiO_3$; $x \sim 20$ nm; $d \sim 280$ nm

Synthesis method	Chemical composition; reaction time; precursor salts	Brief synthesis procedure & heating conditions of processing	Substrate; grain size (x); film thickness (d)
deposition [62]	tetramethyl-3,5-heptanedionate), Fe(III) tris(2,2,6,6-tetramethyl-3,5-heptanedionate), tetraethyl Pb, Ti(IV) t-butoixde, O_2 gas	from Co tris(2,2,6,6-tetramethyl-3,5-heptanedionate), Fe(III) tris(2,2,6,6-tetramethyl-3,5-heptanedionate), tetraethyl lead, titanium (IV) t-butoixde and O_2 gas followed by entering of evaporated precursors into the deposition chamber of MOVCD system. The O_2 flow increased for completion of reactions. The cooling water used to avoid deposition on the walls and to create temperature gradient, and the nanocomposites are kept at room temperature under O_2 gas flow to ensure cooling.	
Off-axis magnetron sputtering and sol–gel spin-coating [63]	NiFe/Pb($Mg_{1/3}Nb_{2/3}$)O_3-$PbTiO_3$; **H**ours	Sol–gel spin coating method used first to deposit PMN-PT films on Pt/Ti/SiO_2/Si substrates, and precursors spin coated at 4000 rpm/30s followed by pyrolyzation at 450°C/5 min. This process was repeated until desired thickness is obtained followed by annealing at 650°C/10 min in air. The sputtering of NiFe thin films on PMN-PT films via off-axis magnetron sputtering at 200°C was the second step. The base pressure of 3×10^{-7} Torr maintained before deposition. The deposition of NiFe thin films was done by applying power of 60 W and Ar gas pressure of 2×10^{-7} Torr.	Pt(111)/Ti/SiO_2/Si; $x \sim$ 10–250 nm; $d \sim$ 30–220 nm
Pulsed laser deposition [64]	**$CoFe_2O_4$-$PbTiO_3$**; **D**ays	Composite targets with preselected fixed compositions used to prepare $CoFe_2O_4$-$PbTiO_3$ thin films. The (001), (110) and (111) $SrTiO_3$ acted as substrate. The 630°C temperature maintained for the substrate and oxygen pressure of 100 mTorr was maintained in the deposition chamber. The approximately 200–230 nm thick films deposited via laser density of 1.6 Jcm^{-2} at a growth rate of 2–3 nm min^{-1}	$SrTiO_3$; x = 50 100 nm $d \sim$ 200–230 nm
Sol–gel followed by dip coating [65]	**$PbTiO_3$/$NiFe_2O_4$**; **H**ours; $Pb(CH_3COO)_2$, Ti$(OC_4H_9)_4$, Ni$(CH_3COO)_2$, $Fe(NO_3)_3$, CH_3COOH, $C_3H_8O_2$	The composition of the raw materials was kept in the mole ratio of Pb:Ti:Ni:Fe of 1:1:1:2 for the final thin film of $PbTiO_3$ and $NiFe_2O_4$. The thin films prepared on silicon substrates using the sol precursor by dip coating, followed by a heat-treatment at 550°C/8 min plus a post heat-treatment at temperatures of 550-950°C/1 h. The acetic acid (CH_3COOH) and ethylene glycol monomethyl ether ($CH_3OCH_2CH_2OH$) acting as solvents during precursor preparation.	Si; x = 80–170 nm; $d \sim$ 1.2 μm
MOD-spin coating [66]	**$Pb_{0.7}Sr_{0.3}(Fe_{0.012}Ti_{0.988})O_3$**; **D**ays;	The precursors solution of $Pb_{0.7}Sr_{0.3}(Fe_{0.012}Ti_{0.988})O_3$ thin film prepared using Pb 2-ethylhexanoate	Pt/Ti/SiO_2/Si; x = 16 nm; d = 500 nm

Synthesis method	Chemical composition; reaction time; precursor salts	Brief synthesis procedure & heating conditions of processing	Substrate; grain size (x); film thickness (d)
	xylene, 2-ethylhexanoic acid, KOH, Pb, Fe, Sr. nitrates, $C_{16}H_{36}O_4Ti$, polyethylene glycol, acetone, isopropanol	$(C_7H_{15}COO)_2Pb$, Sr. 2-ethylhexanoate $(C_7H_{15}COO)_2Sr$, Fe 3-ethylhexanoate and tetra-n-butyl orthotitanate in xylene. An approximately 20 mol% excess of Pb precursor added to compensate for the loss of Pb during heating. The solution refluxed at 110°C with constant stirring for 10 h for homogeneous mixing. The solution spin coated on $Pt/Ti/SiO_2/Si$ substrates by the spin coating technique with 4300 rpm/60s dried at 350°C/5 min to remove the solvent and organic residuals. The final film annealed at 650°C/3 h.	

Bold emphasis has more significance.

Table 3.
Synthesis method used to prepare multiferroic $PbTiO_3$ based thin films.

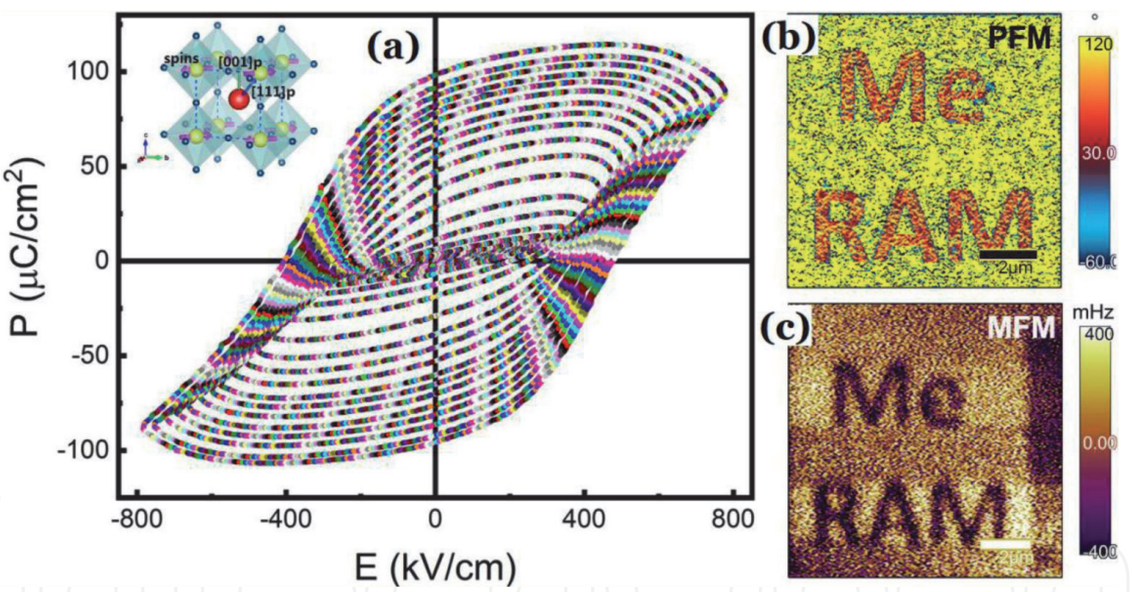

Figure 6.
(a) Spontaneous polarization in $0.85BiTi_{0.1}Fe_{0.8}Mg_{0.1}O_3$–$0.15CaTiO_3$ (BTFM-CTO) thin film. (b) PFM image after electric writing by 10 V, and corresponding. (c) MFM image without an external magnetic field [69].

b = 5.44 Å, c = 7.65 Å) and exhibits cubic ($Pm\bar{3}m$) one above ~1575 K. Below this temperature, CTO has tetragonal (I4/mcm) phase for which transitions of orthorhombic (Pnmb) phase exist below ~1525 K [67]. This orthorhombic structure could create an epitaxial strain in thin films due to changing symmetry at the phase transitions by tilting TiO_6 oxygen octahedral away from cubic one. CTO has possessed its nonpolarity to antiferrodistortive (AFD) distortions of the TiO_6 octahedral rotations and cation displacements that resulting into an orthorhombic (Pbnm) symmetry and $a^- a^- c^+$ rotations in glazer notation [68]. The ferroelectric polarizations and transition temperatures are significantly enhanced in classical ferroelectric perovskite like $BaTiO_3$ and $PbTiO_3$, and the enhancement in lattice strain might to turn ferroelectricity. Otherwise nonpolar ferroelectrics such as $SrTiO_3$ and

$CaTiO_3$ reported strain-induced ferroelectric transition temperatures only at room temperature or below. It is also reported that the simultaneous doping from Ca and Ti ions into $BiFeO_3$ results to decrease electric conductivity and stabilize the polar rhombohedral phase, and the magnetic properties are enhanced by protect oxygen stoichiometry with Fe in +3 oxidation state [68].

2.4.1 Ferroelectricity in $0.85BiTi_{0.1}Fe_{0.8}Mg_{0.1}O_3$-$0.15CaTiO_3$ thin film

Figure 6a shows the ferroelectric polarization (P) for $0.85BiTi_{0.1}Fe_{0.8}Mg_{0.1}O_3$–$0.15CaTiO_3$ thin film at room temperature [69]. This P-E hysteresis loop shows a

Synthesis method	Chemical composition; reaction time; precursor salts	Brief synthesis procedure & heating conditions of processing	Substrate; grain size (x); film thickness (d)
Pulsed laser deposition [69]	**$BiTi_{0.1}Fe_{0.8}Mg_{0.1}O_3$-$CaTiO_3$;** **D**ays; Oxides of Bi, Ti, Fe, Mg, Ca	Conventional solid state reaction method used to synthesize the ceramic target of $0.85BiTi_{0.1}Fe_{0.8}Mg_{0.1}O_3$–$0.15CaTiO_3$. PLD deposition (with the laser source at 355 nm and a repetition rate of 10 Hz) was used to deposit BTFMO thin films on $Pt/TiO_2/SiO_2/Si$ substrate at ~500°C/ 30 min followed by an in-situ thermal annealing process for 10 min and cooled down to room temperature.	$Pt/TiO_2/SiO_2/$ Si; $\boldsymbol{x}$ = 40 nm; $\boldsymbol{d} \sim$ 330 nm
Sol–gel using spin coating [70]	**$BiFeO_3$-$CaTiO_3$;** **H**ours; $Bi(NO_3)_3.5H_2O$, $Fe(NO_3)_3.9H_2O$, $Ca(NO_3)_2.4H_2O$, $[CH_3(CH_2)_3O]_4Ti$	The $Bi(NO_3)_3.5H_2O$ and $Fe(NO_3)_3.9H_2O$ were dissolved in a mixture of 2-methoxy ethanol and ethylene glycol. The acetic anhydride added to the solution in order to acquire pure BFO precursor. An appropriate ratios of $Ca(NO_3)_2.4H_2O$ and $[CH_3(CH_2)_3O]_4Ti$ to obtain BFO-CTO precursor has been prepared. As-synthesized precursor spin coated on $Pt/Ti/SiO_2/Si$ substrates at 3000 rpm/30s and preheated at 350°C/ 10 min, and annealed at 550°C/15 min.	$Pt/Ti/SiO_2/Si$; $\boldsymbol{x}$ = 48–110 nm; $\boldsymbol{d}$ = 300 nm
Sol–gel based solution processing [71]	**$BiTi_{(1-y)/2}Fe_yMg_{(1-y)/2}O_3$–$CaTiO_3$;** **D**ays; Nitrates of Bi, Fe, Mg, Ca $(CH_3COO)_2.H_2O$, $C_{16}H_{36}O_4Ti$, $C_6H_8O_7$, $CH_3OCH_2CH_2OH$ (2MOE), acetic acid and propionic anhydride	Sol–gel precursor solutions prepared by mixing nitrates of Bi, Fe, Mg, Ca $(CH_3COO)_2.H_2O$ and $C_{16}H_{36}O_4Ti$ with $C_6H_8O_7$ and $CH_3OCH_2CH_2OH$ under constant stirring which treated with 2MOE, acetic acid and propionic anhydride. This precursor solution deposited on $SrTiO_3/La_{0.7}Sr_{0.3}MnO_3$ substrate via sol–gel two-step solution processing method.	$SrTiO_3/La_{0.7}Sr_{0.3}MnO_3$; $\boldsymbol{d} \sim$ 30.14 nm
Hydrothermal epitaxy [72]	**$CaTiO_3$;** **D**ay; CaO, TiO_2, KOH	The CaO and TiO_2 were dissolved in a mixture of KOH and H_2O. The solution was put in Teflon-lined autoclave and the substrate put in the bottom of the autoclave, and heated at 200°C/12 h. As-synthesized samples were washed with deionized water and dried in air.	$Nb:SrTiO_3$ (001); $x \sim$ 40 nm; $\boldsymbol{d} \sim$ 350 nm

Bold emphasis has more significance.

Table 4.
Synthesis methods used for fabrication of $CaTiO_3$ based multiferroic thin film.

large remanent polarization of $2Pr = 191.6\ \mu C\ cm^{-2}$ and coercive field (E_c) $2E_c = 681.8\ kV\ cm^{-1}$ without excluding the contribution from the leakage current.

2.4.2 ME coupling in $0.85BiTi_{0.1}Fe_{0.8}Mg_{0.1}O_3$-$0.15CaTiO_3$ thin film

The ME coupling might be studied by considering the magnetic field (H) effect on the ferroelectric polarization and magnetization (magnetic field on the domain switching) that shown in **Figure 6b** and **c** [69]. **Figure 6b** is the PFM image after electric lithography which is observed magnetic domain switching after the electric lithography (**Figure 5c**). Although, the magnetic domains are not completely switched, indicating that the ME coupling is stable at room temperature.

2.4.3 Synthesis techniques for $CaTiO_3$ thin films

Table 4 shown the chemical synthesis methods used in the preparation of multiferroic systems of $CaTiO_3$ thin films.

3. Conclusion and comparative features for synthesis methods used for $BiFeO_3$, $BaTiO_3$, $PbTiO_3$ and $CaTiO_3$ thin films

The chemical synthesis methods for thin film fabrication of perovskite $BiFeO_3$, $BaTiO_3$, $PbTiO_3$ and $CaTiO_3$ multiferroic systems and their composites have been described on the basis of their brief synthesis procedure, time of reaction, composition, heating conditions and morphology. Since thin film composite structures are mostly suitable for chip-device implementation. In various thin film processing methods of multiferroics, the vacuum based deposition like PLD may provide a large ME coupling, enabling the realization of complex microstructures including epitaxy, texture, or columnar distribution of magnetic nanopillars into a ferroelectric matrix. PLD enables the growth of high quality epitaxial thin films with substrate area for coated are small but to the making of uniform films on the wafer level is challenging.

The BFO films made via CSD needs richer oxygen environments for annealing and obtain crystalline films at relatively low temperatures. This CSD method has low cost, easily control of stoichiometry and easy to operate for large area films for a complex-shaped substrates. Among various CSD techniques, polymer assisted deposition (PAD) is most suitable to produce high quality epitaxial complex and multilayer-structured films (film thickness below 100 nm).

The multiferroic thin films deposited with RF sputtering performs high reproducibility with an accurate stoichiometry in a controlled process (but the film growth rate is low and the cost of fabrication is high), and considered to be the most suitable method of thin film preparation due to a smooth surface and dense structure that usable to fabricate the integrated circuit device.

Other chemical synthesis is sol–gel which has good reproducibility, low cost, thickness uniformity and moreover large area deposition and commonly used spin coating deposition. It simply prepared BFO thin films. Photosensitive sol–gel method can integrate the preparation with the fine patterning of the film which can simplify the lithography process remarkably.

The atomic layer deposition (ALD) provides additional degrees of freedom in design and fabrication of devices depending on domain wall optimization, adding the option of conformity in deposition of various geometries (it easily embedded nanoparticles, embedded nanopillars, and nanolaminates according to

configurations, *i.e.* 0–3, 1–3, and 2–2) with unique thickness control and also to fabricate high-quality ultrathin films.

Another chemical technique is the chemical vapor deposition (CVD) which highly usable for BFO thin films deposition which has excellent substrate coverage, low-cost, ease of scale-up, control over thickness and morphology. Aerosol assisted CVD is not rely upon the use of highly volatile precursors, essential for typically high molecular weight heterometallic cluster compounds.

For shape control in multiferroics, hydrothermal method could provide an alternative approach to the synthesis of high-quality epitaxial BFO and BTO thin-film with low-cost. The hydrothermal reaction typically occurs at low temperature (<250°C) and high pressure (<15 MPa) originating from water vapor pressure. The spray pyrolysis method has been implemented for the production of porous and layer by layer films.

Acknowledgements

The author K.C. Verma thankfully acknowledges the financial support by UGC of Dr. DS Kothari Post Doctorate Fellowship [No. F4-2/2006(BSR)/PH/16-17/0066] and CSIR-HRDG for SRA (Pool Scientist) fellowship Grant No. B-12287 [SRA (Pool No): 9048-A].

Author details

Kuldeep Chand Verma[1,2*] and Manpreet Singh[3]

1 Materials Science and Sensor Applications (MSSA), CSIR-Central Scientific Instruments Organisation, Chandigarh, India

2 Department of Physics, Panjab University, Chandigarh, India

3 Department of Chemistry, Eternal University, Baru Sahib, Himachal Pradesh, India

*Address all correspondence to: dkuldeep.physics@gmail.com; kcv0309@gmail.com

References

[1] Ramesh R, Spaldin NA. Multiferroics: progress and prospects in thin films. Nat. Mater. 2007; **6**, 21-29.

[2] Verma KC, Goyal N, Kotnala RK. Tuning magnetism in $0.25BaTiO_3$-$0.75CoFe_2O_4$ hetero-nanostructure to control ferroelectric polarization. Physica B: Conden. Matter. 2019; **554**, 9-16.

[3] Wang J, Neaton JB, Zheng H, Vagarajan V, Ogale SB, Liu B, Viehland D, Vaithyanathan V, Schlom DG, Waghmare UV, paldinNA S, Rabe KM, Wuttig M, Ramesh R. Epitaxial $BiFeO_3$ Multiferroic Thin Film Heterostructures. Science 2003; **299**, 1719-1722.

[4] Chu YH, Martin LW, Holcomb MB, Gajek M, Han SJ, He Q *et al.* Electric-field control of local ferromagnetism using a magnetoelectric multiferroic**.** Nat. Mater. 2008; **7**, 478-482.

[5] Kim DH, Ning S, Ross CA. Self-assembled multiferroic perovskite-spinel nanocomposite thin films: epitaxial growth, templating and integration on silicon. J. Mater. Chem. C 2019; **7**, 9128-9148.

[6] Verma KC, Kotnala RK, Negi NS. Intrinsic study for magnetoelectric coupling in $_{Pb1-x}Srx(Fe_{0.012}Ti_{0.988})O_3$ Nanoparticles. Solid State Commun. 2009; **149**, 1743-1748.

[7] Verma KC, Kotnala RK. Tailoring the multiferroic behavior in $BiFeO_3$ nanostructures by Pb doping. RSC Adv. 2016; **6**, 57727-57738.

[8] Verma KC, Kotnala RK. Multiferroic magnetoelectric coupling and relaxor ferroelectric behavior in $0.7BiFeO_3$-$0.3BaTiO_3$ nanocrystals. Solid State Commun. 2011; **151**, 920-923.

[9] Yin L, Mi W. Progress in $BiFeO_3$-based heterostructures: materials, properties and applications. Nanoscale. 2020; **12**, 477.

[10] Verma KC, Synthesis and Characterization of Multiferroic $BiFeO_3$ for Data Storage. 2020; doi.org/10.5772/intechopen.94049, 106-135.

[11] Zhao T, Scholl A, Zavaliche F, Lee K, Barry M, Doran A, Cruz MP, Chu YH, Ederer C, Spaldin NA, Das RR, Kim DM *et al.* Electrical control of antiferromagnetic domains inmultiferroic $BiFeO_3$ films at room temperature. Nat. Mater. 2006; 5, 823-829.

[12] Bai F. *et al*. Destruction of spin cycloid in $<111>_c$-oriented $BiFeO_3$ thin films by epitaxial constraint: Enhanced polarization and release of latent magnetization. Appl. Phys. Lett. 2005; **86,** 032511.

[13] Gumiel C, Jardiel T, Calatayud DG, Vranken T, Van Bael MK, Hardy A *et al.* Nanostructure stabilization by low-temperature dopant pinning in multiferroic $BiFeO_3$-based thin films produced by aqueous chemical solution deposition. J. Mater. Chem. C. 2020; **8**, 4234-4245.

[14] Jalkanen P, Tuboltsev V, Marchand B, Savin A, Puttaswamy M, Vehkamaki M *et al.* Magnetic Properties of Polycrystalline Bismuth Ferrite Thin Films Grown by Atomic Layer Deposition. J. Phys. Chem. Lett. 2014; **5**, 4319-4323.

[15] Waghmare SD, Jadhav VV, Shaikh SF, Mane RS, Rhee JH, O'Dwyer C. Sprayed tungsten-doped and undoped bismuth ferrite nanostructured films for reducing and oxidizing gas sensor applications. Sens. Act. A. 2018; **271**, 37-43.

[16] Tomczyk M, Bretos I, Jimenez R, Mahajan A, Ramana EV, Calzada ML *et al.* Direct fabrication of $BiFeO_3$ thin

films on polyimide substrates for flexible electronics. **J. Mater. Chem. C**. 2017; **5**, 12529-12537.

[17] Moniz SJA, Cabrera RQ, Blackman CS, Tang J, Southern P, Weaverd PM *et al.* A simple, low-cost CVD route to thin films of $BiFeO_3$ for efficient water photo-oxidation. J. Mater. Chem. A. 2014; **2**, 2922-2927.

[18] Palgrave RG, Parkin IP. Aerosol Assisted Chemical Vapor Deposition Using Nanoparticle Precursors: A Route to Nanocomposite Thin Films. J. Am. Chem. Soc. 2006; **128**, 1587-1597.

[19] Tiwari D, Fermin DJ, Chaudhuri TK, Ray A, Solution Processed Bismuth Ferrite Thin Films for All-Oxide Solar Photovoltaics. J. Phys. Chem. C 2015; **119**, 5872-5877.

[20] Zargazia M, Entezari MH, A novel synthesis of forest like $BiFeO_3$ thin film: Photo-electrochemical studies and its application as a photocatalyst for phenol degradation. Appl. Surf. Sci. 2019; **483**, 793-802.

[21] Castro A, Martins MA, Ferreira LP, Godinho M, Vilarinho PM, Ferreira P, Multifunctional nanopatterned porous bismuth ferrite thin films. J. Mater. Chem. C. 2019; **7**, 7788-7797.

[22] Lee TK, Sung KD, Jung JH, Electric polarization and diode-like conduction in hydrothermally grown $BiFeO_3$ thin films, J. Alloys Compd. 2015; **622**, 734-737.

[23] Wang Z, Li Y, Viswan R, Hu B, Harris VG, Li J, Viehland D. Engineered Magnetic Shape Anisotropy in $BiFeO_3$-$CoFe_2O_4$ Self-Assembled Thin Films. ACS Nano. 2013; **7(4)**, 3447-3456.

[24] Han H, Lee JH, Jang HM. Low-Temperature Solid-State Synthesis of High-Purity $BiFeO_3$ Ceramic for Ferroic Thin-Film Deposition. Inorg. Chem. 2017; 56(**19**), 11911-11916.

[25] Azeem W, Riaz S, Bukhtiar A, Hussain SS, Xu Y, Naseem S. Ferromagnetic ordering and electromagnons in microwave synthesized $BiFeO_3$ thin films. J. Magn. Magn. Mater. 2019; **475**, 60-69.

[26] Islam MR, Zubair MA, Bashar MS, Rashid AKMB. $Bi_{0.9}Ho_{0.1}FeO_3/TiO_2$ Composite Thin Films: Synthesis and Study of Optical, Electrical and Magnetic Properties. Sci. Rep. 2019; **9**: 5205.

[27] Yan F, Zhao G, Song N, Zhao N, Chen Y. In situ synthesis and characterization of fine-patterned La and Mn co-doped $BiFeO_3$ film. J. Alloys Compd. 2013; **570**, 19-22.

[28] Vila-Fungueirino JM, Gomez A, Antoja-Lleonart J, Gazquez J, Magen C, Noheda B *et al.* Direct and Converse Piezoelectric Responses at the Nanoscale from Epitaxial $BiFeO_3$ Thin Films Grown by Polymer Assisted Deposition. **Nanoscale**. 2018; **10**, 20155-20161.

[29] Pham CD, Chang J, Zurbuchen MA, Chang JP. Synthesis and Characterization of $BiFeO_3$ Thin Films for Multiferroic Applications by Radical Enhanced Atomic Layer Deposition. Chem. Mater. 2015; 27, **21**, 7282-7288.

[30] Kim TC, Ojha S, Tian G, Lee SH, Jung HK, Choi JW *et al.* Self-assembled multiferroic epitaxial $BiFeO_3$-$CoFe_2O_4$ nanocomposite thin films grown by rf magnetron sputtering. J**. Mater. Chem. C**, 2018; **6**, 5552-5561.

[31] Simoes AZ, Riccardi CS, Santos MLD, Garcia FG, Longo E, Varela JA. Effect of annealing atmosphere on phase formation and electrical characteristics of bismuth ferrite thin films. Mater. Res. Bull. 2009; **44**, 1747-1752.

[32] Bretos I, Jimenez R, Ricote J, Sirera R, Calzada ML. Photoferroelectric Thin Films for Flexible Systems by a

Three-in-One Solution-Based Approach. Adv. Funct. Mater. 2020, **30(32)**, 2001897.

[33] Das S, Basu S, Mitra S, Chakravorty D, Mondal BN. Wet chemical route to transparent $BiFeO_3$ films on SiO_2 substrates. Thin Solid Films 2010; **518**, 4071-4075.

[34] Guo H, Zhao R, Jin K, Gu L, Xiao D, Yang Z *et al.* Interfacial-Strain-Induced Structural and Polarization Evolutions in Epitaxial Multiferroic $BiFeO_3$ (001) Thin Films. ACS Appl. Mater. Interf. 2015; **7**, 2944-2951.

[35] Wang L, Wang Z, Jin KJ, Li JQ, Yang HX, Wang C *et al.* Effect of the Thickness of $BiFeO_3$ Layers on the Magnetic and Electric Properties of $BiFeO_3/La_{0.7}Sr_{0.3}MnO_3$ Heterostructures. Appl. Phys. Lett. 2013; **102**, 242902.

[36] Verma KC, Kotnala RK. Multiferroic approach for Cr,Mn,Fe,Co,Ni,Cu substituted $BaTiO_3$ Nanoparticles. Mater. Res. Express 2016; 3, 055006.

[37] Verma KC, Kotnala RK. Lattice Defects Induce Multiferroic Responses in Ce, La-Substituted $BaFe_{0.01}Ti_{0.99}O_3$ Nanostructures. J. Am. Ceram. Soc. 2016; 99[5], 1601-1608.

[38] Verma KC, Singh D, Kumar S, Kotnala RK. Multiferroic effects in $MFe_2O_4/BaTiO_3$ (M = Mn, Co, Ni, Zn) Nanocomposites. J. Alloys Compd. 2017; **709**, 344-355.

[39] Lu X, Kim Y, Goetze S, Li X, Dong S, Werner P *et al.* Magnetoelectric Coupling in Ordered Arrays of Multilayered Heteroepitaxial $BaTiO_3/CoFe_2O_4$ Nanodots. Nano Lett. 2011; **11**, 3202-3206.

[40] Stanescu D, Magnan H, Sarpi B, Rioult M, Aghavnian T, Moussy JB *et al.* Electrostriction, Electroresistance, and Electromigration in Epitaxial $BaTiO_3$-Based Heterostructures: Role of Interfaces and Electric Poling. ACS Appl. Nano Mater. 2019; **2**, 3556-3569.

[41] Khan S, Humera N, Niaz S, Riaz S, Atiq S, Naseem S. Simultaneous Normal – Anomalous Dielectric Dispersion and Room Temperature Ferroelectricity in CBD Perovskite $BaTiO_3$ Thin Films. J Mater Res Technol. 2020; **9**, 11439-11452.

[42] Dai YQ, Dai JM, Tang XW, Zhang KJ, Zhu XB, Yang J *et al.* Thickness Effect on the Properties of $BaTiO_3$-$CoFe_2O_4$ Multilayer Thin Films Prepared by Chemical Solution Deposition. J. Alloys Compd. 2014; **587**, 681-687.

[43] Alberca A, Munuera C, Azpeitia J, Kirby B, Nemes NM, Perez-Munoz AM, Tornos J, Mompean FJ, Leon C, Santamaria J, Garcia-Hernandez M. Phase Separation Enhanced Magneto-Electric Coupling in $La_{0.7}Ca_{0.3}MnO_3/BiTiO_3$ Ultra-Thin Films. Sci Rep. 2015; **5**, 17926.

[44] Jiang G, Zhou D, Yang J, Shao H, Xue F, Fu Q. Microstructure and Multiferroic Properties of $BaTiO_3/CoFe_2O_4$ Films on Al_2O_3/Pt Substrates Fabricated by Electrophoretic Deposition. J. Eur. Cer. Soc. 2013; **33**, 1155-1163.

[45] Erdem D, Bingham NS, Heiligtag FJ, Pilet N, Warnicke P, Vaz CAF *et al.* Nanoparticle-Based Magnetoelectric $BaTiO_3$— $CoFe_2O_4$ Thin Film Heterostructures for Voltage Control of Magnetism. ACS Nano. 2016; **10**, 9840-9851.

[46] Tang Y, Wang R, Zhang Y, Xiao B, Li S, Du P. Magnetoelectric Coupling Tailored by the Orientation of the Nanocrystals in One Component in Percolative Multiferroic Composites. RSC Adv. 2019; **9**, 20345.

[47] Mudiyanselage RRHH, Magill BA, Burton J, Miller M, Spencer J, McMillan

K *et al.* Coherent Acoustic Phonons and Ultrafast Carrier Dynamics in Hetero-Epitaxial $BaTiO_3$–$BiFeO_3$ Films and Nanorods. J. Mater. Chem. C. 2019; **7**, 14212.

[48] Yan LH, Liang WZ, Liu SH, W Huang, Lin Y. Multiferroic $BaTiO_3$-$CoFe_2O_4$ Nano Composite Thin Films Grown by Polymer-Assisted Deposition. Integ. Ferr. 2011; **131**, 82-88.

[49] Gao X, Zhang D, Wang X, Jian J, He Z, Dou H, Wang H. Vertically Aligned Nanocomposite $(BaTiO_3)_{0.8}$: $(La_{0.7}Sr_{0.3}MnO_3)_{0.2}$ Thin Films with Anisotropic Multifunctionalities. Nanoscale Adv. 2020; **2**, 3276.

[50] Sun Y, Zhang L, Wang H, Guo M, Lou X, Wang D. Excellent Thermal Stability of Large Polarization in $(Bi_{0.5}Na_{0.5})$ TiO_3-$BaTiO_3$ Thin Films Induced by Defect Dipole. Appl. Surf. Sci. 2019; **504**, 144391.

[51] Kawamura G, Oura K, Tan WK, Goto T, Nakamura Y, Yokoe D *et al.* Nanotube Array-Based Barium Titanate-Cobalt Ferrite Composite Film for Affordable Magnetoelectric Multiferroics. J. Mater. Chem. C. 2019; **7**, 10066-10072.

[52] Zhou L, Fu Q, Xue F, Tang X, Zhou D, Tian Y *et al.* Multiple Interfacial Fe_3O_4@$BaTiO_3$/P(VDF-HFP) Core-Shell-Matrix Films with Internal Barrier Layer Capacitor (IBLC) Effects and High Energy Storage Density. ACS Appl. Mater. Interf. 2017; **9**, 40792-40800.

[53] Verma KC, Kotnala RK, Ram M, Negi NS. Optical Characteristics of Nanocrystalline $Pb_{1-x}Sr_xTiO_3$ Thin Films Using Transmission Measurements. Adv. Sci. Focus 2012; 1(1), 1-7.

[54] Verma KC, Shah J, Kotnala RK. Strong Magnetoelectric Coupling of $Pb_{1-x}Sr_x(Fe_{0.012}Ti_{0.988})O_3$ Nanoparticles. J. Nanosci. Nanotechnol. 2015; 15(2), 1587-1590.

[55] Bhatti HS, Hussain ST, Khan FA, Hussain S. Synthesis and Induced Multiferroicity of Perovskite $PbTiO_3$; A review. Appl. Surf. Sci. 2016; **367**, 291-306.

[56] Verma KC, Negi NS. Magnetoelectric coupling and relaxor ferroelectric properties of $Pb_{0.7}Sr_{0.3}(Fe_{0.012}Ti_{0.988})O_3$ thin film. Scr. Mater. 2010; **63**, 891-894.

[57] Verma KC, Singh M, Kotnala RK, Negi NS. Ferromagnetism and ferroelectricity in highly resistive $Pb_{0.7}Sr_{0.3}(Fe_{0.012}Ti_{0.988})O_3$ nanoparticles and its conduction by variable-range-hopping mechanism. Appl. Phys. Lett. 2008; 93, 072904.

[58] Sakamoto W, Iwata A, Moriya M, Yogo T. Electrical and magnetic properties of Mn-Doped $0.7BiFeO_3$-$0.3PbTiO_3$ Thin Films Prepared Under Various Heating Atmospheres. Mater. Chem. Phys. 2009; **116**, 536-541.

[59] Gopman DB, Chen P, Lau JW, Chavez AC, Carman GP, Finkel P *et al.* Large Interfacial Magnetostriction in $(Co/Ni)_4$/ $Pb(Mg_{1/3}Nb_{2/3})O_3$–$PbTiO_3$ Multiferroic Heterostructures. ACS Appl. Mater. Interf. 2018; **10**, 24725-24732.

[60] Zhang P, Gao C, Lv F, Wei Y, Dong C, Jia C *et al.* Hydrothermal Epitaxial Growth and Nonvolatile Bipolar Resistive Switching Behavior of $LaFeO_3$-$PbTiO_3$ Films on Nb: $SrTiO_3$(001) Substrate. Appl. Phys. Lett. 2014; **105**, 152904.

[61] Murakami M, Chang KS, Aronova MA, Lin CL, Yu MH, Simpers JH *et al.* Tunable Multiferroic Properties in Nanocomposite $PbTiO_3$-$CoFe_2O_4$ Epitaxial Thin Films. Appl. Phys. Lett. 2005; **87**, 112901.

[62] Pan M, Liu Y, Bai G, Hong S, Dravid VP, Petford-Long AK. Structure-Property Relationships in Self-

Assembled Metalorganic Chemical Vapor Deposition–Grown $CoFe_2O_4$–$PbTiO_3$ Multiferroic Nanocomposites Using Three Dimensional Characterization. Appl. Phys. Lett. 2011; **110**, 034103.

[63] Feng M, Hu J, Wang J, Li Z, Shu L, Nan CW. Converse Magnetoelectric Coupling in Ni Fe/Pb $(Mg_{1/3}Nb_{2/3})$ O_3–$PbTiO_3$ Nanocomposite Thin Films Grown on Si Substrates. Appl. Phys. Lett. 2013; **103**, 192903.

[64] Levin I, Li J, Slutsker J, Roytburd AL. Design of Self-Assembled Multiferroic Nanostructures in Epitaxial Films. Adv. Mater. 2006; **18**, 2044-2047.

[65] Zhu L, Dong Y, Zhang X, Yao Y, Weng W, Han G et al. Microstructure and Properties of Sol-Gel Derived $PbTiO_3/NiFe_2O_4$ Multiferroic Composite Thin Film with the Two Nano-Crystalline Phases Dispersed Homogeneously. J. Alloys Compd. 2010; **503**, 426-430.

[66] Kotnala RK, Verma KC, Mathpal MC, Negi NS. Multifunctional behaviour of nanostructured $Pb_{0.7}Sr_{0.3}(Fe_{0.012}Ti_{0.988})O_3$ thin film. J. Phys. D: Appl. Phys. 2009; **42**, 085408.

[67] Haislmaier RC, Lu Y, Lapano J, Zhou H, Alem N, Sinnott SB *et al.* Large tetragonality and room temperature ferroelectricity in compressively strained $CaTiO_3$ thin films. APL Mater. 2019; **7**, 051104.

[68] Karpinsky DV, Troyanchuk IO, Sikolenko V, Efimov V, Kholkin AL. Electromechanical and magnetic properties of $BiFeO_3$-$LaFeO_3$-$CaTiO_3$ ceramics near the rhombohedral-orthorhombic phase boundary. J. Appl. Phys. 2013; **113**, 187218.

[69] Jia T, Fan Z, Yao J, Liu C, Li Y, Yu J *et al.* Multi-Field Control of Domains in A Room Temperature Multiferroic $0.85BiTi_{0.1}Fe_{0.8}Mg_{0.1}O_3$-$0.15CaTiO_3$ Thin Film. ACS Appl. Mater. Interf. 2018; 10**(24)**, 20712-20719.

[70] Wu X, Kuang D, Yao L, Yang S, Zhang Y. The Structural, Optical, Ferroelectric Properties of (1-x) $BiFeO_3$-$xCaTiO_3$ Thin Films by a Sol–Gel Method. J Mater Sci: Mater Electron. 2017; 28, 493-500.

[71] Liu C, An F, Gharavi PSM, Lu Q, Zha J, Chen C *et al.* Large-Scale Multiferroic Complex Oxide Epitaxy with Magnetically Switched Polarization Enabled by Solution Processing, Natl. Sci. Rev. 2020; **7**, 84-91.

[72] LV F, Gao C, Zhang P, Dong C, Zhang C, Xue D. Bipolar Resistive Switching Behavior of $CaTiO_3$ Films Grown by Hydrothermal Epitaxy. RSC Adv. 2015; **5**, 40714-40718.